2-14-2014

A Study on the Mechanical Characteristics of a Fiberglass Bed Formed During a Loss-of-Coolant-Accident at a PWR Nuclear Facility

Kyle Hammond

Kyle Hammond
Candidate

Mechanical Engineering
Department

This thesis is approved, and it is acceptable in quality and form for publication:

Approved by the Thesis Committee:

Dr. Arsalan Razani , Chairperson

Dr. Yu-Lin Shen

Dr. Kerry Howe

Dr. Edward Blandford

Dr. Seung-Jun Kim

A Study on the Mechanical Characteristics of a Fiberglass Bed Formed During a Loss-of-Coolant-Accident at a PWR Nuclear Facility

by

Kyle Hammond

B.S., Mechanical Engineering, New Mexico State University, 2011

THESIS

Submitted in Partial Fulfillment of the

Requirements for the Degree of

Master of Science

Mechanical Engineering

The University of New Mexico

Albuquerque, New Mexico

December, 2013

Dedication

I dedicate this thesis to my God who has blessed me with abilities to succeed in engineering, my parents, Asa and Cara Hammond who always pushed me to reach my goals, academically and non-academically, and my wife, Tasha who is someone who always encourages and supports me.

Acknowledgments

First, I would like to thank Cody for all the effort in helping me construct and complete my experiments, you have been invaluable. I would also like to thank the rest students of my group for all their support, Lana, Chris, Kody, Niko, and Sterling. You all helped me in some capacity with my thesis and I am very thankful. I would also like to thank my PI, Dr. Howe. You have always humored my countless visits to your office and pointed me in the right direction time after time. I would like to thank my new PI's, Dr. Kim and Dr. Blandford, your advice and guidance has been truly helpful. Finally, I would like to thank the UNM Mechanical Engineering Department and my adviser Dr. Razani, I have learned a lot in my two years here, and am proud to now not only be an Aggie, but also a Lobo.

A Study on the Mechanical Characteristics of a Fiberglass Bed Formed During a Loss-of-Coolant-Accident at a PWR Nuclear Facility

by

Kyle Hammond

B.S., Mechanical Engineering, New Mexico State University, 2011
M.S., Mechanical Engineering, University of New Mexico, 2013

Abstract

Following a Loss-of-Coolant-Accident (LOCA) in one of the primary coolant lines in the containment building of a PWR Facility, it is possible that fiberglass pipe insulation could be dislodged and washed down to the sump pool. This fiberglass could collect into a "bed" and cause blockage on the sump screens, preventing the emergency re-circulation pumps from operating correctly. GSI-191 is a Nuclear Regulatory Commission (NRC) initiative to understand the effects a sump blockage would have on emergency cooling systems. Recently, the focus has been on understanding how the fiberglass bed will behave during an accident. An attempt was made to classify physical properties of the fiberglass bed that will allow for prediction of head loss through these beds. The analysis of experimental data successfully produced the Hammond Fiberglass Head-Loss (HFH) correlation. The HFH correlation predicts head-loss through an NEI fiberglass bed using only the fiber bed mass and the velocity through the bed. The HFH correlation has allowed for better understanding

of fiberglass bed mechanics through its approach at assuming a non-uniform bed porosity, something that has not been done to this point.

Contents

List of Figures

List of Tables

Glossary

Blenderized	Fiberglass prepared in a blender
GSI-191	NRC Generic Safety Issue 191
HFH	Hammond Fiberglass Head-Loss Correlation
LANL	Los Alamos National Laboratory
LOCA	Loss-of-Coolant-Accident
NEI	Nuclear Energy Institute (fiber)
NPSH	Net-Positive-Suction-Head
NRC	Nuclear Regulatory Commission
PNNL	Pacific Northwest National Laboratory
PWR	Pressurized Water Reactor
SSFEL	Small-Scale-Fiber-Evaluation-Loop
STP	South Texas Project
S_v	Specific Surface Area
ϵ_m	Mixed Bed Porosity

Glossary

ϵ	Bed Porosity
μ	Dynamic Viscosity
ν	Kinematic Viscosity
U, v, w_A	Bed Approach Velocity
$\Delta H, dP, P_{HL}$	Head-Loss
$\Delta L_o, L$	Fiberglass Bed Thickness
dz	Incremental Fiberglass Bed Thickness
ρ	Fluid Density
K_1, K_2, K	Ergun Constant
V_{void}	Volume of Liquid in a Fiberglass Bed
Vol_{bed}, V_{total}	Total Volume of a Fiberglass Bed Including Fiber and Liquid
ρ_{bulk}	Bulk Density
m, m_{fiber}	Fiberglass Bed Mass
m_{sp}	Specific Mass of Fiberglass Bed
H_{tap}	Height to Tap Measured from Bottom Screen
$H_{bed}, \frac{\rho_L}{m_{sp}}$	Height to Top of Fiberglass Bed Measured from Bottom Screen
RL, z_r	Relative Location
LD, ρ_L	Linear Density
d, d_p	Diameter of a Fiberglass Fiber
SA_{screen}	Surface Area of the Sump Strainer or Testing Screen

Chapter 1

Introduction and Background

1.1 Introduction

The goal of this thesis is to investigate the mechanical behavior of various types of fiberglass materials present after an LOCA (Loss-of-coolant-accident) scenario by fitting the Ergun coefficients and developing a fiberglass bed porosity-depth function for various types of fiberglass and system conditions. The fiberglass is thought to arrange itself in a bed on the sump re-circulation screens following a LOCA. The Ergun coefficients are measured for the fiberglass material when it is arranged in a fiber bed (porous bed), similar to the one shown in Figure 1.2. This bed will be subject to varying degrees of fluid flow, varying methods of fiber preparation, and various amounts of fiber glass material used to generate the bed. The way in which this fiber bed behaves under these fluid flow conditions will in turn affect the total pressure drop across the fiber bed and the calculated Ergun coefficient. Another aspect of developing a better understanding of fiber bed behavior during an accident scenario is understanding the depth (in a bed) vs. porosity relationship as a function of system conditions (velocity, mass of bed, height of bed, etc.). This

porosity relationship will be explored and used in the Ergun equation to model head-loss across the bed more accurately. The head-loss experienced across the bed is important because the emergency sump re-circulation pumps, downstream of the fiber bed, have a fixed NPSH (Net Positive Suction Head) requirement, under which they will no longer operate correctly or may fail altogether. The overall goal of the experiments is to experimentally extract flow material properties (Ergun coefficients and porosity relationships) for different types of fiberglass beds subject to varying flow conditions found during an LOCA event.

1.2 The Loss-of-Coolant-Accident (LOCA)

A LOCA can occur in many areas of a nuclear reactor. The scope of this study will address LOCA's occurring in the main hot and cold leg coolant lines coming and going from the reactor vessel. The coolant lines are typically filled with water and are charged to thousands of psi. The LOCA of interest involves the rupture of one of these coolant lines, involving a material failure on the piping wall that results in the spilling of highly charged (high pressure), two-phase coolant out of the pipe into the containment building. The spraying of highly charged coolant into the containment building is what initiates the accident scenario of interest.

Generic Safety Issue - 191 (GSI-191) addresses the potential for highly charged coolant jetted from a pipe during a LOCA to damage thermal insulation used in the containment building [2]. Once the thermal insulation is damaged, it may separate and wash down to the bottom of the containment building where the re-circulation pumps are located downstream of sump screens. The sump screens are designed to prevent large debris from entering the flow channel upstream of the re-circulation pumps. If the re-circulation pumps become damaged, the primary cooling mechanism for the plant during a LOCA could be lost. The NRC initiated the study of GSI-191

with a brief study of the parameters at all United States Nuclear Power Plants related to GSI-191 [3]. This study generated key information that was used by Los Alamos National Laboratory (LANL) in subsequent studies involving debris generation [5], transport, and capture on the sump screens. Throughout the evolution of GSI-191, it became clear that investigation into fiberglass debris, generated from a LOCA that damages thermal insulation on pipes, would be a primary area of research.

1.3 The Fiberglass Bed

As mentioned previously, it is postulated that during a LOCA, chunks of fiberglass insulation will break off of piping after being exposed to a high-pressure jet of coolant. These chunks, of varying sizes, will then wash down through the plant into the sump pool. Figure 1.1 shows sources of debris in the containment building; they are indicated by arrows. It is believed that once the fiber washes down into the

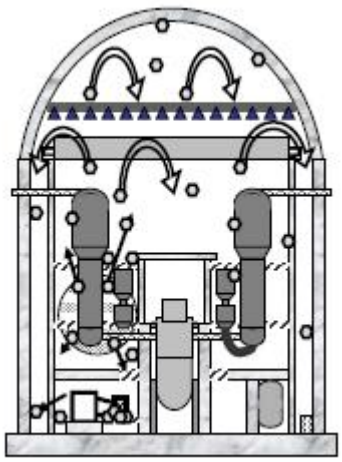

Figure 1.1: Fiberglass debris sources inside containment for a PWR

sump pool that it will begin to migrate towards the sump screens located at the

bottom of the pool. The transport of the fiberglass material in the sump pool was previously researched by Maji et al [5]. The results showed that fiberglass debris could accumulate near or on the sump screens and thicknesses of 2 to 6-in could be observed [5]. The fiberglass "bed" will be composed of the fiberglass debris that accumulates on the sump screen. This debris bed will look something like Figure 1.2. Figure 1.2 shows a debris bed used in the UNM CHLE test [4]. It is composed of a

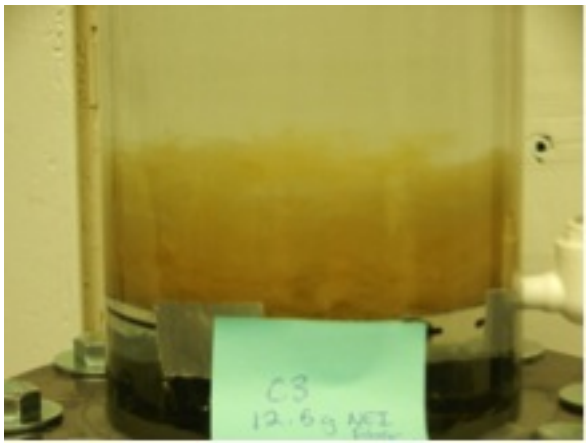

Figure 1.2: Fiberglass inside a test column for UNM CHLE test. The fiber is suspended in water and being held up by a stainless steel screen located at the bottom of the fiberglass bed.

perforated stainless steel screen and processed fiberglass, which represents the STP (South Texas Project) sump screens and fiberglass debris, respectively. The debris bed was formed by pouring fiber into the top of the UNM CHLE test column and allowing it to settle in the flow of water at a prescribed velocity, onto the screen. The UNM CHLE test columns can be seen in Figure 1.3.

Figure 1.3: UNM CHLE test column set up. Fiberglass is introduced through the top most flange. [4]

1.4 Previous Work Conducted on Fiberglass Debris Beds

Both experimental and analytical work has been conducted in the area of fiberglass bed characterization. Most analytical work has yet to be properly verified through experiments due to the uniqueness and difficulty of measuring certain material properties to a high accuracy of a porous media that is highly compressible (fiberglass bed).

1.4.1 Experimental Work

CR-6224 Correlation

The most widely known model for predicting head-loss through a fiberglass bed is the CR-6224 correlation developed for the Nuclear Regulatory Commission in 1995 [10]. The correlation is of the modified Ergun Equation type and aims to predict head-loss across a bed by fitting parameters a_0, b_0, and ϵ_m such that

$$\frac{\Delta H}{\Delta L_0} = (a_0 S_v^2 (1-\epsilon_m)^{1.5}(1+57(1-\epsilon_m)^3))\mu U + b_0 \frac{S_v(1-\epsilon_m)}{\epsilon_m}\rho U^2)\frac{\Delta L_m}{\Delta L_0} \quad (1.1)$$

where,

$a_0 = 1.435 * 10^{-4}(\frac{ft-water/in}{lbm/ft^2 s^2})$

$b_0 = 2.741 * 10^{-5}(\frac{ft-water/in}{lbm/ft^2 s^2})$

S_v is the specific surface area (ft^2/ft^3)

μ is dynamic viscosity $(lbm/s-ft)$

U is velocity (ft/s)

ΔH is head loss $(ft-water)$

ρ is water density (lbm/ft^3)

ΔL_0 is the fiber bed theoretical thickness

ΔL_m is the actual fiber bed thickness

ϵ_m is mixed bed porosity

The correlation was used as an estimator to predicting head-loss through a fiberglass bed following a LOCA, however, the equation fails to address something very important. Equation 1.1 treats porosity as a constant through the bed. This is a good estimate for very thin beds, however, if a fiberglass bed becomes thick enough, it is hypothesized that there will be a non-uniform porosity distribution through the bed, parallel to flow. The porosity distribution through a bed is one parameter that

will be studied in this thesis. The 6224 Correlation is supposed to apply to all types of fiberglass, shredded, NEI, blender, and mixed particulate beds assuming uniform thickness and composition.

PNNL Blender Research

Further research done on bed behavior was performed by Pacific Northwest Laboratory (PNNL) in 2006 [9]. The researchers were primarily focused on the preparation techniques used to create a blenderized fiberglass bed of NUKON fiberglass. A Blenderized fiber bed is prepared by taking fiberglass cubes (1 inch on each side) from a sheet of fiberglass, placing the cubes in a blender container with water, and blending the fiberglass on the chop setting of the blender for a prescribed time. Their work was based on the current head loss correlation of the time developed for GSI-191 scenarios, the 6224 Correlation [10]. PNNL experimented with varying techniques for generating blenderized fiber that encompassed various blender times, amounts of liquid (water based) solution in the blender, and amounts of fiberglass in the blender. This approach yielded basic material properties for the blenderized fiberglass, however, PNNL did not address NEI fiberglass, which is made from the same fiberglass cubes but instead of placing in a blender the cubes are placed in a bucket at subjected to pressure washer spray, or a less chopped, on the order of twenty seconds, blenderized fiberglass that is being used in current UNM testing [6]. PNNL was also testing fiberglass bed properties at flow velocities greater than 0.1 ft/s. During PNNL testing, nuclear power plants did have designed sump screen approach velocities greater than 0.1 ft/s, however, recently many plants redesigned their sump screens to lower the approach velocity. South Texas Project's sump screens have an approach velocity of 0.01 ft/s, putting them potentially in a different flow regime (turbulent vs. laminar) than previous experimental work performed [6].

UNM Work

There has also been a heavy focus on how chemical precipitates could become clogged in a fiber bed during a LOCA. These precipitates, or solids, are hypothesized to be produced from corrosion occurring throughout the inside of the containment building during a LOCA. It is theorized that once these precipitates capture on the fiberglass bed formed on the sump screen, that head loss will increase very quickly and cause a pump failure at the plant. UNM has been focusing on testing this theory with the current series of CHLE tests. These tests have aimed to determine if corrosion products will induce a head loss across a fiberglass bed. One outcome of the UNM testing has been a concern that the fiberglass bed, NEI and blenderized, is not well understood. If the way a fiberglass bed behaves without any precipitate is not understood, then there is no way of knowing the exact effects of chemical precipitates on head loss across a fiber bed.

UNM Fiberglass Preparation Techniques

Previous work on GSI-191 has aimed to solve the problem of pressure loss through a fiberglass bed after a LOCA. Even though much work has been done for all aspects of this problem, there is still not a general consensus as to what the fiberglass will look like after it has been destroyed by the water jet, washed down through the containment building, and accumulated on the sump screens. Previous testing has used fiber that is of the blenderized and NEI type. The blenderized fiber is usually prepared by taking Nukon fiberglass sheets that are several inches thick, cutting them into small cubes, usually about 1 x 1 x 1 inches, and placing them in a standard food blender, filled with Borated TSP (Trisodium Phosphate) water [12] for a specified time. The longer the fiberglass is in the blender, the finer the fiber will become. Figure 1.4 shows fiberglass on a light table after it has been blended. Notice how

Figure 1.4: Blenderized fiberglass sample from a UNM CHLE test.

small (short) the fibers are. The second type of fiberglass used is known as NEI fiber. NEI fiber was developed by the Nuclear Energy Institute (NEI) for the purpose of GSI-191 [15]. NEI fiber is prepared by taking and cutting similar size chunks from the sheet of Nukon fiberglass as the blenderized technique, but instead of placing the fiberglass in the blender it is placed in a bucket where it is sprayed with Borated-TSP water from a pressure washer at approximately 1800 psi until the fiber becomes very stringy. Figure 1.5 shows the NEI fiber placed against a light table. In comparison

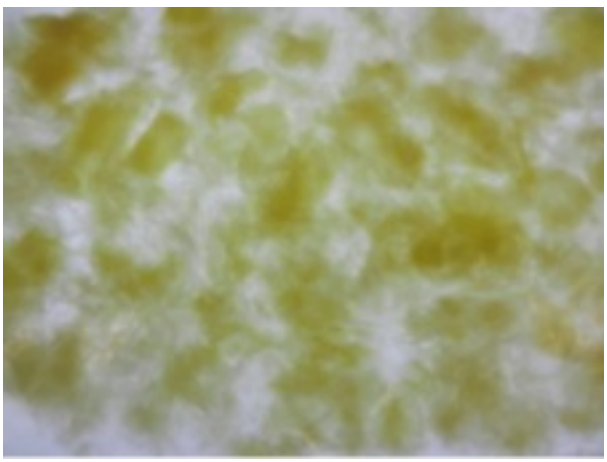

Figure 1.5: NEI fiberglass sample from a UNM CHLE test.

to the blenderized fiber shown in Figure 1.4, the NEI fiber in Figure 1.5 is much chunkier and less processed. As one would expect, both of these fibers will behave differently under flow conditions in the sump pool and ultimately on the sump screen. Their physical characteristics, fiber length being the most distinguishable, will likely affect how tightly they pack, how they rearrange themselves under flow conditions, and how much debris they capture during a LOCA. The two fiber types, blenderized and NEI, represent the types of fiber currently being tested for the GSI-191 effort. It is the purpose of this thesis to determine how varying types of Fiberglass categorized under NEI Fiber behave mechanically and structurally. NEI is believed to be the most likely type of fiber found after an LOCA. Since it is currently impractical to perform a large scale test at a nuclear power plant to determine what the NEI fiberglass debris would look like once it reaches the sump screen, understanding the properties of different types of fiberglass allows for one to project bed behavior and ultimately, pressure loss through the debris bed, for multiple scenarios (types of NEI).

1.4.2 Analytical Work

Dr. Bruce Letellier of Los Alamos National Lab (LANL), attempted to describe fiberglass beds analytically. Dr. Letellier indicated that the pressure loss at any point in the fiberglass bed would be dependent on three terms: the shear force, the drag force, and other forces that arise from the assumption that spatial gradients exist in all the physical variables [1]. His equation proposes that pressure loss through a fiberglass bed is composed to three components, shear, drag, and other forces.

$$-\left(\frac{dP}{dz}\right)_{Total} = -\left(\frac{dP}{dz}\right)_{Shear} - \left(\frac{dP}{dz}\right)_{Drag} - \left(\frac{dP}{dz}\right)_{Other} \tag{1.2}$$

Equation 1.2 allows porosity to be treated as a function of depth (z) as shown in Equation 1.3

$$\Delta P_{Shear} = 2\mu w_A \int_{top}^{bot} S_v^2 \frac{(1-\epsilon)^2}{\epsilon^3} dz \tag{1.3}$$

This aligns with the field of thought this thesis will implement, that porosity is a function of depth.

1.5 Ergun Equation Coefficients

The Ergun equation was first formulated by Sabri Ergun in 1952 [7]. The modified Ergun Equation is shown below in Equation 1.4:

$$\frac{\Delta P}{L} = K_1 \frac{(1-\epsilon)^2 \rho \nu U}{\epsilon^3 d^2} + K_2 \frac{(1-\epsilon)\rho U^2}{\epsilon^3 d} \tag{1.4}$$

where, ΔP is the pressure drop across the bed, L is the bed length, ϵ is the bed porosity, ρ is the fluid density, ν is the kinematic viscosity of the fluid, U is superficial flow velocity, d is particle diameter, and K_1 and K_2 are physical constants to be determined [8]. To further simplify the problem, the K_2 term will be eliminated. It is theorized that since, for this experiment, velocities U, will be on the order of 0.1 ft/s or less and d will be 7.1 μm (fiberglass diameter), such that the U^2 can be ignored since the Particle Reynolds Number, shown in Equation 1.5

$$Re = \frac{\rho U d_{fiber}}{\mu} \tag{1.5}$$

will be less than 1 [13].

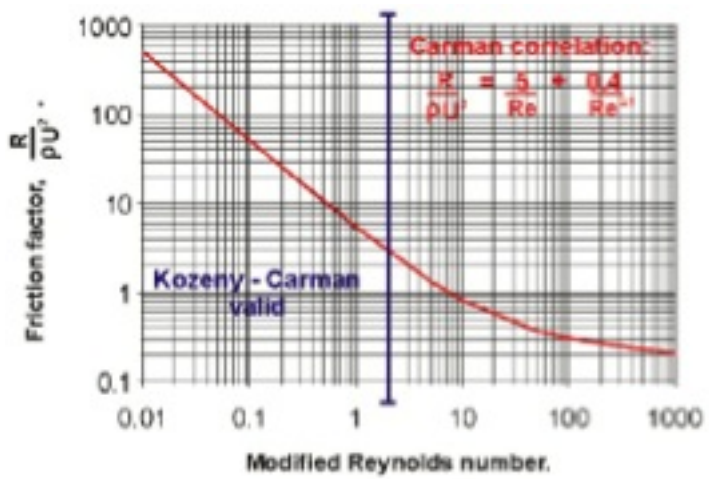

Figure 1.6: Where the Carman-Kozeny equation is valid

Figure 1.6 shows where the Carman-Kozeny equation (first term of the Ergun equation) is valid. That leaves the simplified version of Equation 1.6:

$$\frac{\Delta P}{L} = K\frac{(1-\epsilon)^2 \rho \nu U}{\epsilon^3 d^2} \tag{1.6}$$

where K is the only variable typically solved for.

Chapter 2

Methods

2.1 Introduction

This chapter will outline the methods utilized during experimentation. It will also briefly describe the types of experiments that occurred, with further detail in the results section. All experiments were conducted at the UNM CHLE Test Facility as seen in Figure 2.1.

Figure 2.1: UNM CHLE Testing Facility in Albuquerque New Mexico

2.2 Fiber Preparation

Fiberglass preparation techniques have been controversial within the GSI-191 field for quite some time. There has not been a consensus as to how one would emulate fiberglass following a LOCA at a PWR facility. Many types of fiberglass preparation techniques have been proposed, shredded [10], blenderized [2], and NEI [11]. NEI fiberglass has been hypothesized to model post-LOCA fiberglass the best, and as such will be used for the purpose of this research [6].

Fiberglass sheets are found in many PWR's wrapped around coolant lines. These sheets help boost the plants thermal efficiency. This is the source of fiberglass for GSI-191 testing. These sheets are typically NUKON Fiberglass Sheets [14], manufactured my PCI Engineering. The Nukon Sheets come in varying thicknesses with a bulk sheet density of $2.4\frac{lb_m}{ft^3}$ [15]. The individual fiber density is $175\frac{lb_m}{ft^3}$ [15]. Fiberglass

Figure 2.2: Nukon Fiberglass with one side "baked" (upper brown part)

sheets are exposed to very high temperatures when wrapped around the coolant pipe which causes them to become "baked" on the side exposed to the pipe surface. This phenomena is matched for experimentation by literally baking one side of fiberglass and producing what is seen in Figure 2.2. It is not known, nor has it been studied, if baked fiberglass behaves differently than non-baked fiberglass. What is known is that at high temperature, the bonding agent in the sheet breaks down and alters the fiberglass sheet structure at some level [16]. All experiments are performed with a fiberglass mix from both the baked (brown) and non-baked (yellow) portion of the fiberglass sheet. When making NEI fiber, the first step is to cut chunks of fiberglass from a sheet to the desired mass. The fiber is then cut into approximately 1"x1"x1" cubes and placed into a bucket with the fiber nearly submerged in water, as seen in Figure 2.3. The fiberglass is then sprayed with a high power pressure washer at over 1000 psi. The pressure washer wand is placed in the bucket and the fiber is sprayed (below the water surface) as seen in Figure 2.4. This spray treatment lasts for approximately 1 minute. The resulting fiberglass, now NEI, can be seen in Figure

Figure 2.3: Nukon Fiberglass 1” cubes submerged in tap water

2.5. This NEI fiberglass is now ready for introduction in to the test column utilizing loading techniques outlined in a subsequent section.

Figure 2.4: NEI Fiberglass being made by spraying with a pressure washer

Figure 2.5: NEI Fiberglass submerged in tap water

2.3 Apparatus

The apparatus consists of both existing CHLE infrastructure and newly built equipment. The primary use of existing infrastructure was to provide pumping power for the new Small-Scale-Fiber-Evaluation-Loop (SSFEL). The pumping power would come from column 3 of the CHLE setup. The connections between column 3 of CHLE and the SSFEL are seen in Figure 2.6. SSFEL has the ability to run fiberglass characterization tests very quickly and efficiently due to its design. It is designed to test pressure drop across the fiberglass bed utilizing a differential pressure cell (online). Velocity in the loop is controllable by a Variable Frequency Drive (VFD), used to control the pump. The SSFEL also has the capability to compress fiberglass beds mechanically with a compression screen. A diagram of the SSFEL is pictured in Figure 2.7. The SSFEL's compression mechanism is shown schematically in Figure 2.8. Figure 2.8 shows before and after the compression of a fiberglass bed. The com-

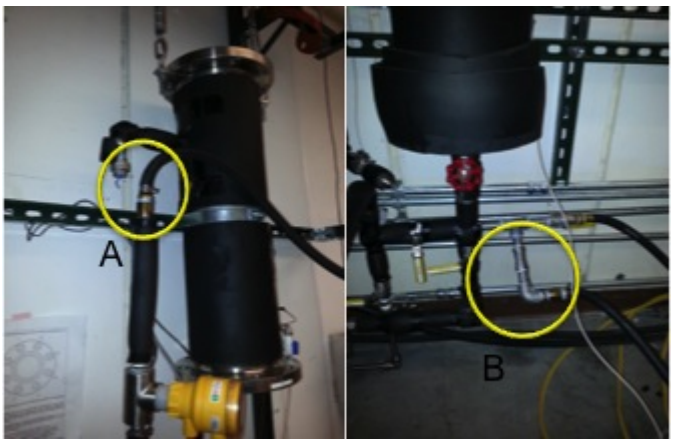

Figure 2.6: Connections between CHLE Column 3 and the SSFE Loop. "A" shows flow from the pump, through the flow meter, to the inlet side of the SSFEL. "B" shows the return from the outlet of the SSFEL to the pumping section in CHLE Column 3.

pression screen's primary purpose is to control the porosity of the bed by changing the volume of the bed. Porosity is defined as

$$\epsilon = \frac{V_{Void}}{V_{Total}} \tag{2.1}$$

where, V_{Void} is the volume of liquid in the bed and V_{Total} is the total volume of liquid and solids in the bed. The compression screen has the ability to alter the volume of liquid in the bed, when the fiber bed is defined as the space between the purple and red screen in Figure 2.7. The final build of SSFEL can be seen in Figure 2.9. The SSFEL can test fiber beds ranging in thickness from less than an inch all the way up above 3 feet. This capability is very useful to understanding bed behavior. It is believed that beds of great thickness (3 feet) have not been tested before. Halfway through testing, SSFEL was equipped with a new manometer tube column to allow for expanded measurement capabilities. The new column tube allowed for pressure to be measured incrementally throughout the bed by utilizing pressure taps placed

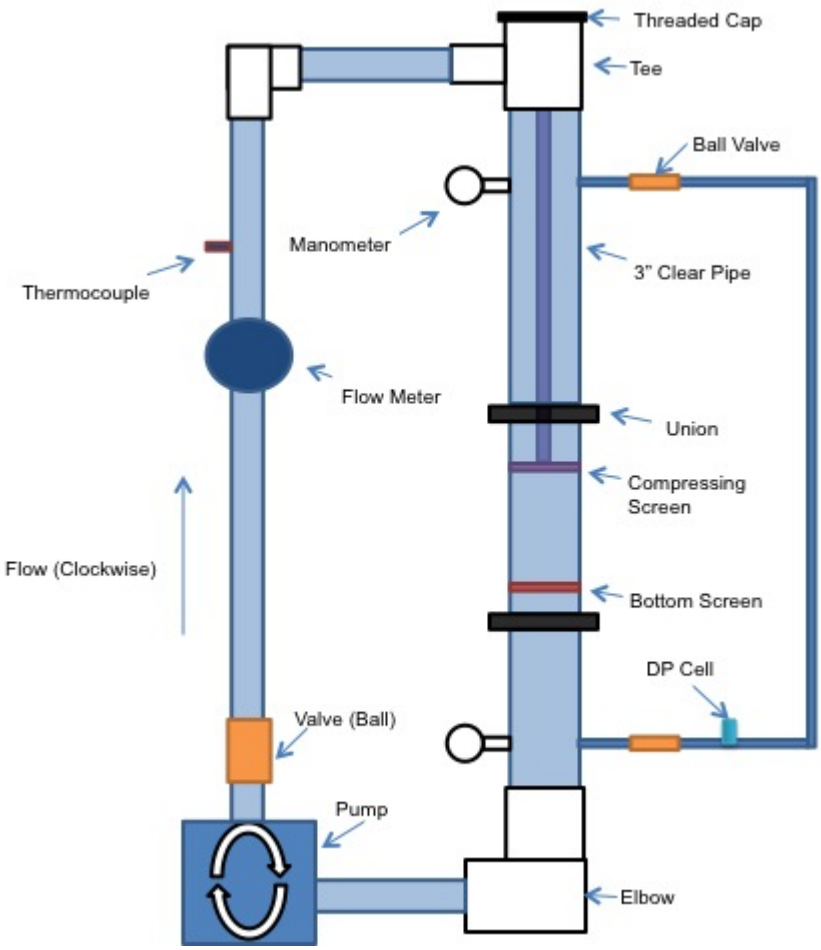

Figure 2.7: SSFEL Schematic

1" apart starting from the bottom screen and continuing upward. The new column can be seen in Figure 2.10.

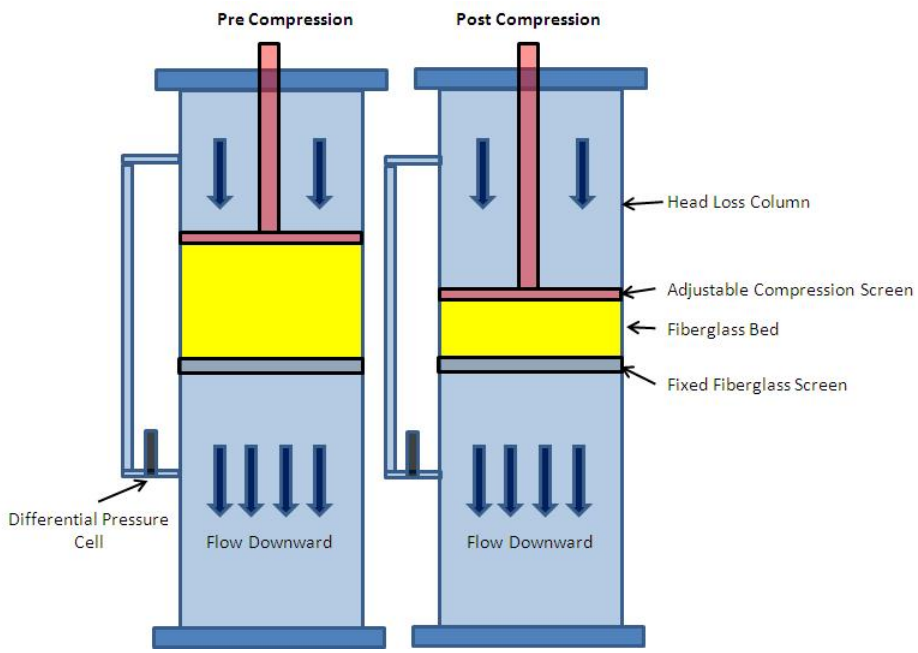

Figure 2.8: Fiberglass Head Loss Testing Column Setup.

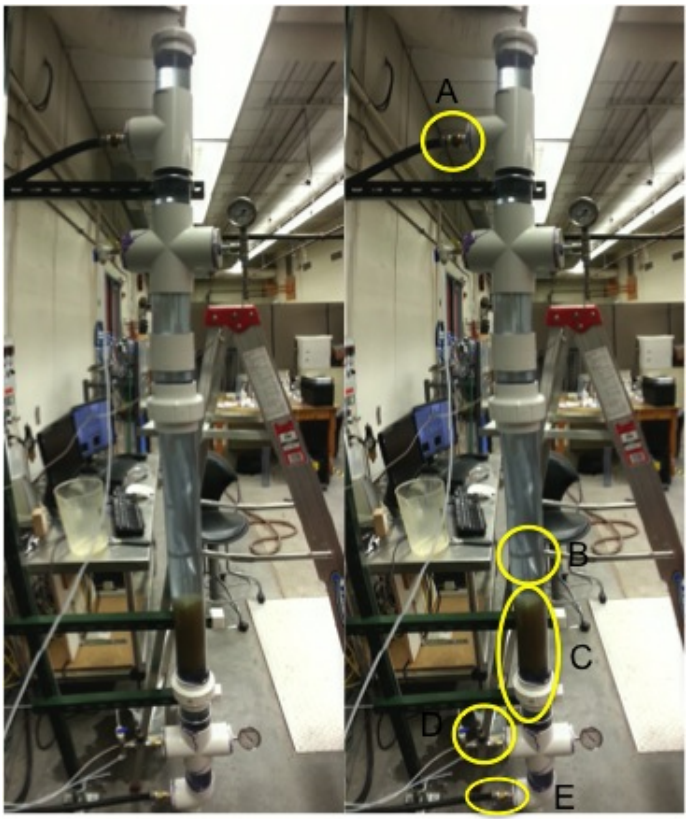

Figure 2.9: (Left) SSFEL apparatus. (Right) "A" is the flow inlet from the pump, "B" is the compression screen, "C" is the fiberglass bed, "D" is the Differential Pressure cell, and "E" is the return to the pump. Flow is from top to bottom.

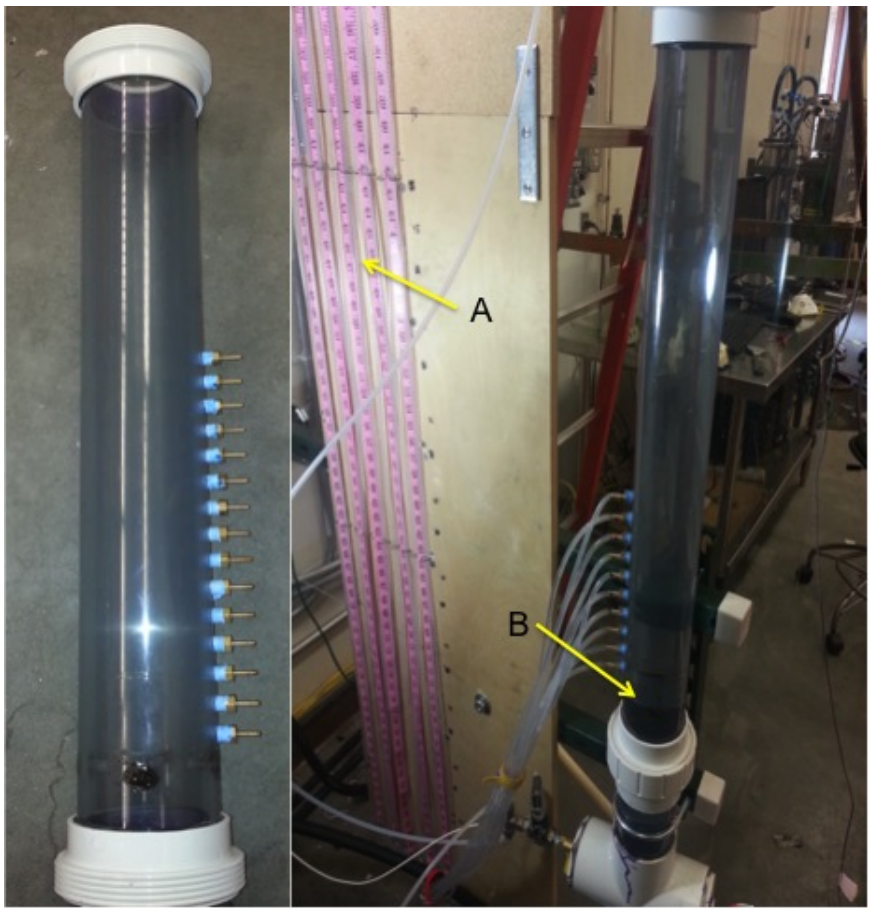

Figure 2.10: The manometer column is seen on the left. The manometer column setup is seen on the right. "A" is the manometer tubing and readings as measured by tape measures. "B" is the bottom of the screen or bottom of the fiberglass bed when loaded.

2.4 Fiber Loading

Once fiberglass has been processed from its original sheet state to NEI it is placed in a beaker full of water and ready for loading into the column. Figure 2.11 shows the NEI fiberglass prepared for loading. The column will first be prepped for experimentation by throttling the flow to the appropriate loading velocity as defined by the experimental plan, for most tests this is around 0.1 ft/s. Once the column is at a steady state flow condition, two experimenters will climb on ladders, straddling the top of the SSFEL, and begin slowly pouring fiberglass out of beaker into the testing column. It is very important to pour fiber at a constant rate so that loading can be consistent between subsequent tests. Once all of the fiber from the beaker

Figure 2.11: NEI fiberglass ready to be introduced to the testing column

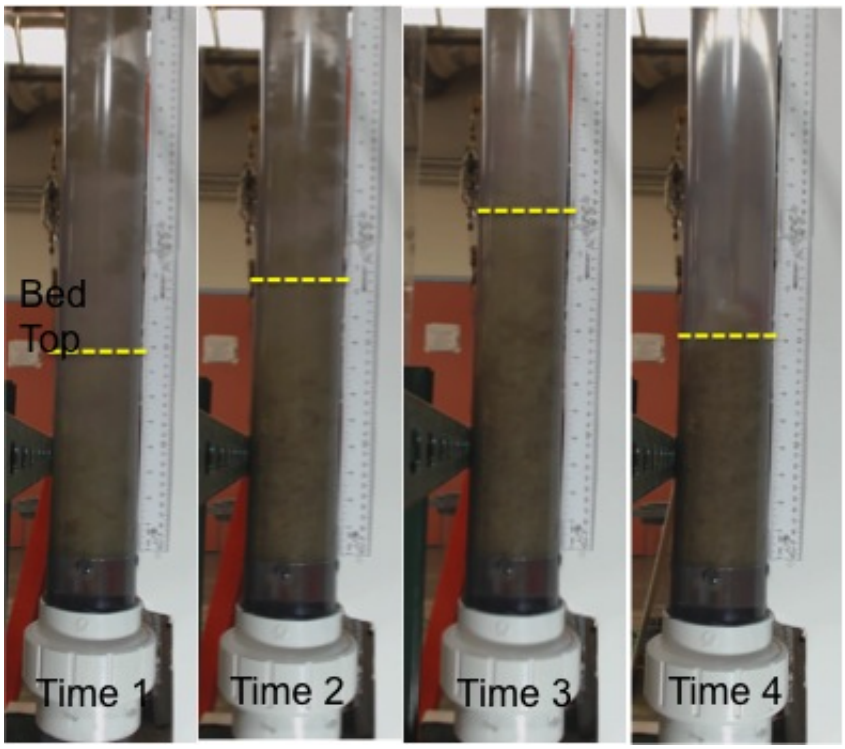

Figure 2.12: NEI fiberglass bed loading at 0.1 ft/s. Time is increasing from left to right with approximate bed height at each time marked by the horizontal line. Time 1 corresponds to just after fiber introduction begins and Time 4 corresponds to steady-state. Flow is from top to bottom.

is exhausted, the fiber is allowed to self load and slowly compact until it reaches steady-state. Typically, a fiber bed will grow taller during the loading stage, but then compact to a smaller steady-state height once it has settled upon itself. This phenomena of a growing bed followed by the steady-state relaxation can be seen in Figure 2.12. Once the fiberglass bed has been loaded, it will then be ready for experimentation. Experiments may consist of varying the velocity or compressing the fiber manually or by flow. All fiberglass bed heights are recorded using a stand with a permanent measuring device which is placed next to the column during testing.

2.5 Instrumentation

The SSFEL is instrumented to measure flow rate, pressure loss via a differential pressure transducer, pressure via manometer tubing, temperature, and bed height. It also can control velocity in the column and take readings using a LabView module. The mass of the fiberglass is taken using a counter-top scale. Calibrations have been performed on the flow meter, pressure transducer, thermocouple, and counter-top scale.

Flow Meter

The flow meter used in the SSFEL is the same used in UNM CHLE testing [6]. It is and OMEGA FMG-3002-PP-D flow meter. It is a 1/2" ID flow meter that was calibrated and measured to less than 2 percent error. The flow meter can be seen in Figure 2.13.

Figure 2.13: OMEGA FMG-3002-PP-D flow meter used during testing

Pressure Transducer

The differential pressure transducer used is an MMDWUOOSV1OP3C6T2A4CE from OMEGA. It is rated from 0-5 psi which corresponds to 0-138.35 in. H2O. The transducer is accurate within 0.05 percent at 72 Degrees F., which is near the operating temperature for testing. The pressure transducer can be seen in Figure 2.14.

Figure 2.14: SSFEL Differential Pressure Transducer

Thermocouple

The thermocouple used for experimentation is an OMEGA 5TC-TT-K-20-36. It has a measured error of $\pm 0.843\,^{\circ}\mathrm{C}$.

Remaining Instruments

The resolutions for measurements of the remaining instruments are the manometer tubing measurement devices ($\pm\frac{1}{16}$ in. H2O resolution), the bed height measuring device ($\pm\frac{1}{16}$ in. H2O resolution), a Metler Toledo table-top scale ((± 0.1 g resolution), and Hitachi VFD's that control the pump motors to the 0.01th Hz. (range 0-60 Hz.)

Chapter 3

Results

Experiments were performed in accordance with the goal of characterizing NEI fiberglass bed properties under post-LOCA flow conditions. The following results reflect different aspects of the bed behavior and answer distinct questions about fiber behavior under certain conditions. Each experimental purpose will be detailed in it's respective section.

3.1 NEI Fiber Preparation Utilizing Varying Nozzles

Currently, NEI fiber is prepared using cubes of fiberglass (1" on each side) that, when placed in a bucket, are blasted with 1800 psi water for approximately one minute. Previous to UNM CHLE testing [6], NEI was not characterized by the type of nozzle tip that was used on the pressure washer when blasting the fiberglass. UNM decided to be consistent and use a 40° tip. What was not understood is how the angle of the nozzle tip affects the hydraulic response of the NEI bed. This test was designed to

compare different preparation techniques for NEI fiberglass using 0, 15, 25, and 40 degree nozzles. A single 40g batch of NEI fiberglass was made using each of the four nozzles. The different NEI fiberglass samples can be seen on a light table according to its nozzle angle in Figure 3.1.

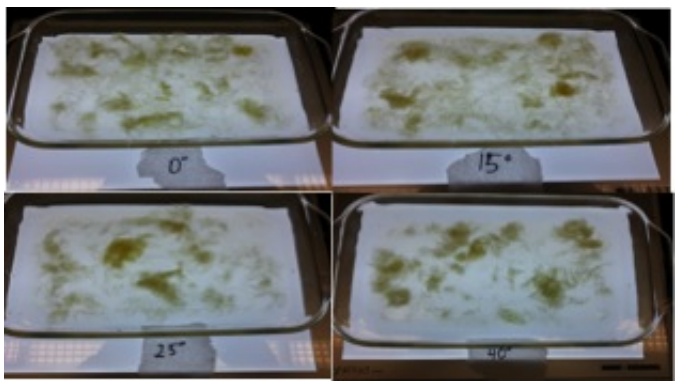

Figure 3.1: Fiber Results from the Varying Nozzle Angle Placed on a Light Table

The fiberglass beds were then loaded into the testing column at 0.085 ft/s. The 0 and 40 degree beds were loaded at 0.085 ft/s then the velocity was lowered to 0.04 ft/s then 0.02 ft/s. The velocity was then raised back up at each point it came down, generating a velocity "sweep". 15 and 25 degree fiberglass beds were loaded at 0.085 ft/s and a single pressure reading was taken. In all cases the bed was allowed to reach steady-state at the prescribed flow conditions before a pressure reading was recorded. The results from the test can be seen below in Figure 3.2. The results show that, in general, the fiberglass beds behaved relatively the same. Each bed responded hydraulically (head-loss) nearly the same. The only relationship that may exist is, that if you group together 0 and 15 degree and 25 and 40 degree fiber, it can be seen that the first group, 0 an 15 degree fiber, typically produce lower head-loss readings than that of the second group. This is likely caused by 0 and 15 degree fiber being more pulverized (less clumpy) than 25 and 40 degree fiber. When fiber is more clumpy it has pockets of highly compressed fiber. More compressed fiber will

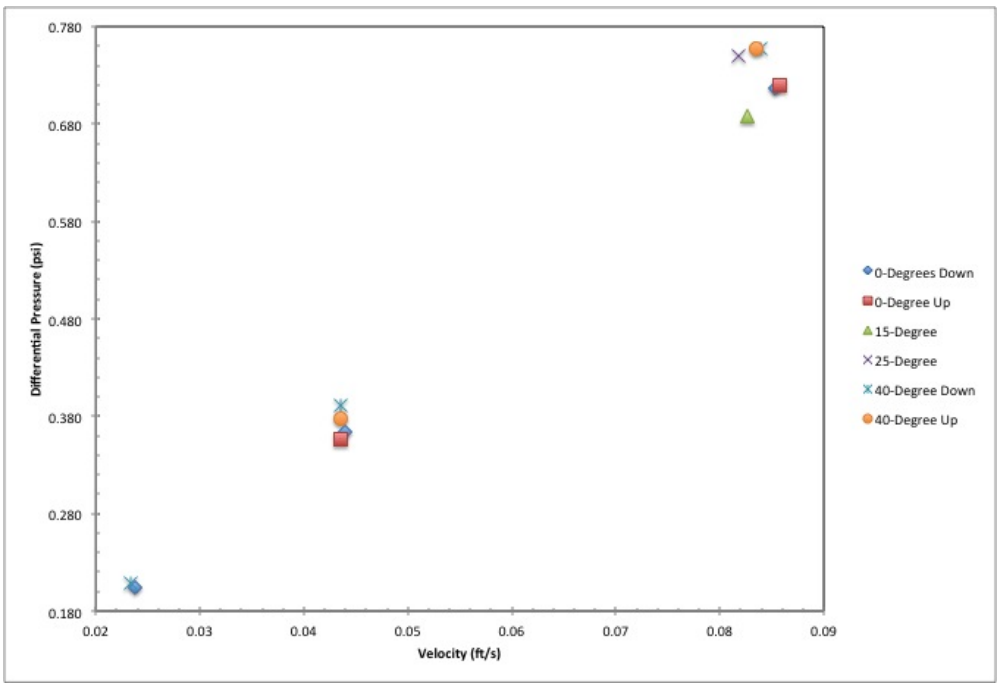

Figure 3.2: Head-loss response of a 40 gram fiberglass bed prepared with different pressure washer nozzle angles

lead to greater head-loss. This is why the next test, the NEI compression test, is used to measure the head-loss response characteristics of 0 and 15 degree fiber vs. 25 and 40 degree fiber subjected to artificial compression.

3.2 NEI Compression and Velocity Variation with 15 and 40 Degree Fiber

After the "NEI Fiber Preparation Utilizing Varying Nozzles" test was performed, it was decided that a more in depth look at how NEI fiberglass preparation (nozzle type) affects bed behavior. The starting point for this test was to group the nozzles used in the previous test into two categories, 0 and 15 degrees, and 25 and 40 degree.

These two categories of nozzles produced similar head-loss characteristics (within each respective category). It was chosen to use 15 degree NEI and 40 degree NEI for this test. Each nozzle would be used to generate three NEI beds, an 40 gram bed, an 80 gram bed, and an 120 gram bed. Each distinct bed would be subject to varying velocity and compression (by the fiberglass compression screen). The fiberglass compression screen controls a value known as bulk density. Bulk density of a fiberglass bed is defined as the mass of the bed divided by the total volume the bed occupies, including fiber and water. Bulk density is

$$\rho_{bulk} = \frac{m_{fiber}}{Vol_{bed}} \tag{3.1}$$

The beds were loaded at a prescribed velocity with the compression screen not in place. The velocity was then lowered in steps and then raised back up to the initial loading velocity. Once back at loading velocity, the compression screen is lowered 10 percent of the original bed height and the sweep is repeated. This process is repeated in increments of 10 percent all the way to 50 percent of original height. The final compression height is known as "max compression" and is the height at which the experimenter could not compress the bed further. Figure 3.3 shows the progression of the compression's through a test.

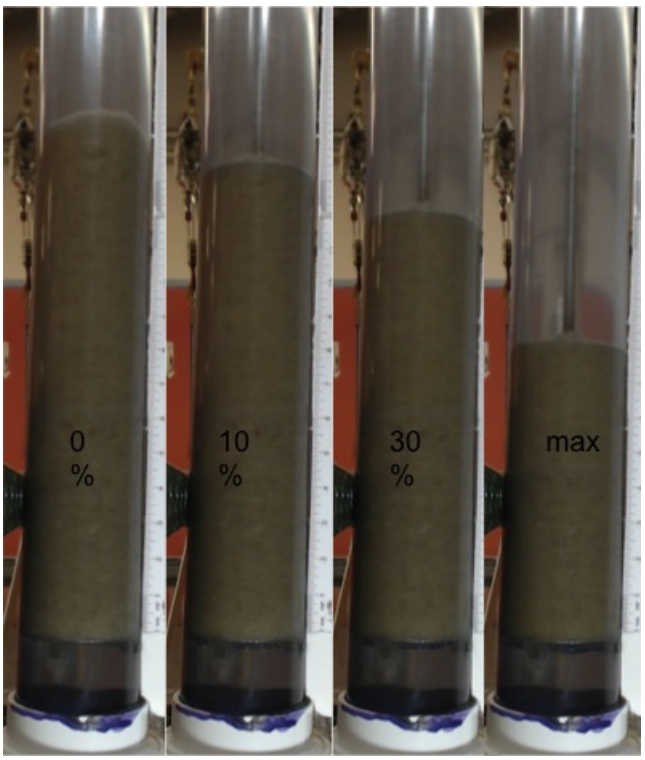

Figure 3.3: An example of the compression screen at various compression percentages for a NEI 120g 15 deg bed

40 gram NEI Bed

First, in Figure 3.4, is the results of the NEI 40g 15 deg vs. 40 deg test. The test is conducted at various velocities and compression levels (bulk density).

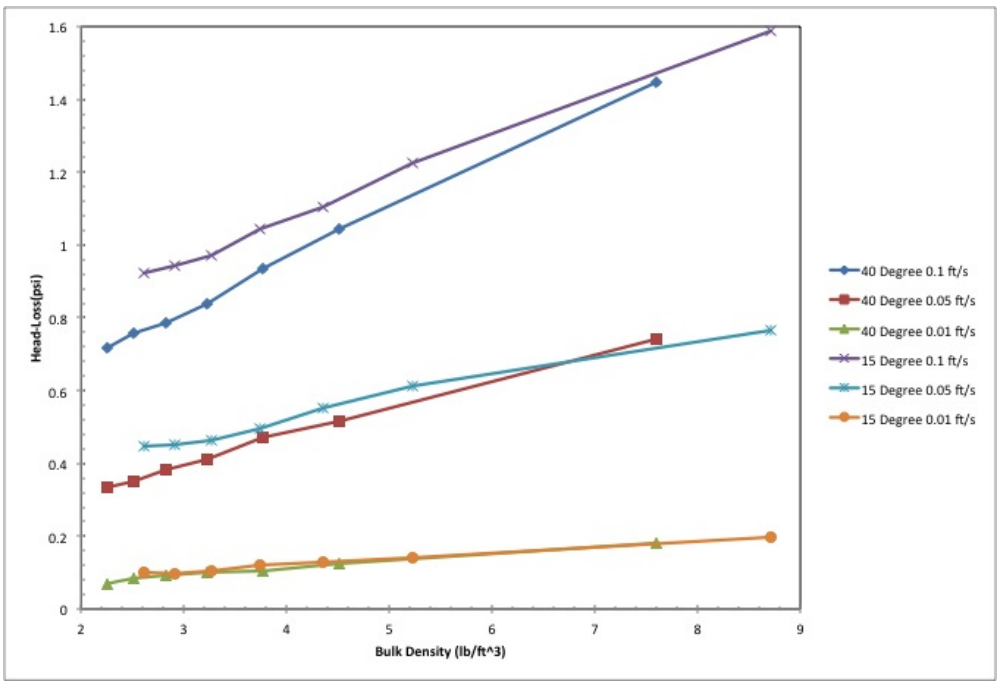

Figure 3.4: Results for the NEI 40g 15 deg vs. 40 deg test. Both beds are subject to varying velocity and compression

The results from Figure 3.4 indicate that at lower velocities 15deg and 40deg fiber head-loss readings agree more than they do at higher velocities. This is represented by the 0.01 ft/s lines being nearly on top of each other. As velocity increases, the difference between the two nozzle angle beds increases. The difference between the two angles is characterized by a difference in vertical translation of differential pressure reading and slope. It is also worth noting that the initial bed height, 8 inches for the 15 degree fiber and 9.5 inches for the 40 degree fiber may affect the results. Bed formation height is affected by how clumpy the fiberglass is. Because the 15 degree fiber had a lower formation height, it shows that its bed is more tightly packed (less clumpy), because there is less void space in the 15 degree bed, it makes sense why it would, in general, experience greater head-loss than the 40 degree bed.

80 gram NEI Bed

Figure 3.5 shows the results for the NEI 80g 15 deg vs. 40 deg test.

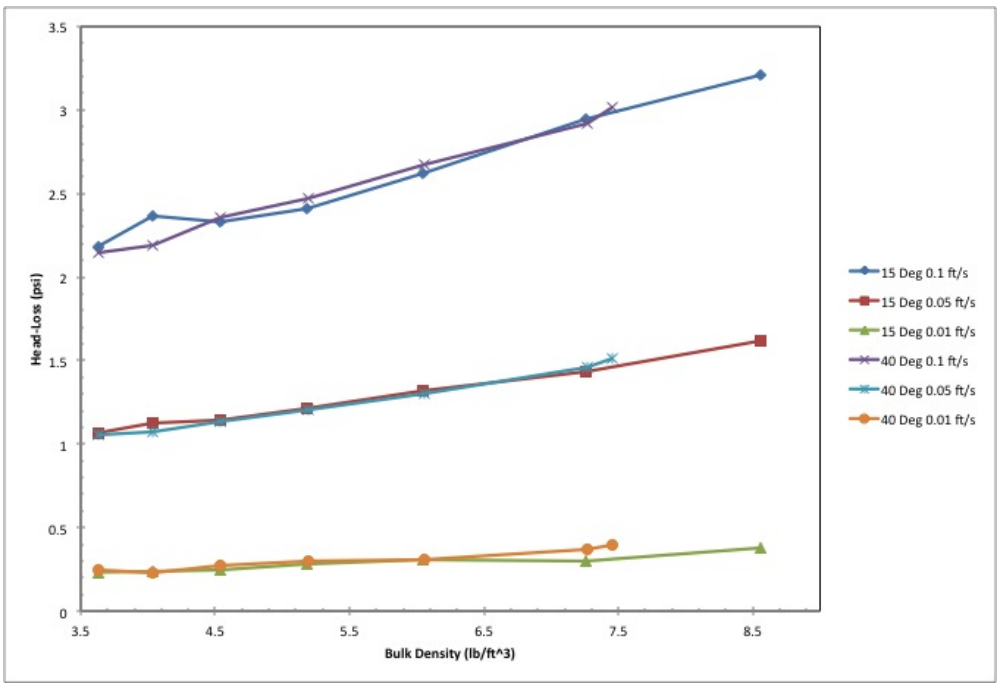

Figure 3.5: Results for the NEI 80g 15 deg vs. 40 deg test. Both beds are subject to varying velocity and compression

The results from the 80g test show that head-loss characteristics between 15 deg and 40 deg fiber are nearly identical. This is in contrast to the 40g test. This is likely due to the increase in homogeneity of the bed during formation as the mass of the bed increases. With more mass comes more force on bottom portions of the bed due to more weight of fiber above and more drag on the fiber above inducing a force on bottom sections of the bed. More compression forces on the bottom of the bed will cause the bed to fill void spaces, increasing the homogeneity of the bed. It may also be a function of the head-loss reading, as the 40g bed was generally lower than 1 psi of head-loss and the 80g bed is generally greater than 1 psi of head-loss at the

higher two velocities.

120 gram NEI Bed

The last test for this series was with a 120g fiberglass bed. This bed was not compressed at as many intervals as previous beds because the head-loss was approaching the upper limits of safe operation of the differential pressure transducer. The results can be seen below in Figure 3.6. The results of the 120g test agree with the 80g test.

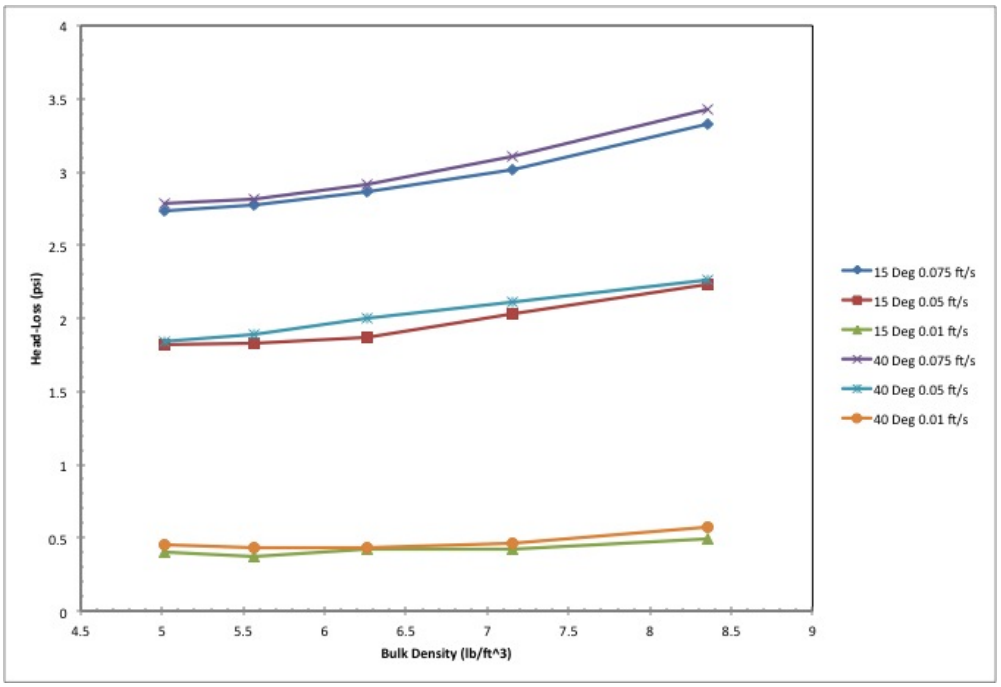

Figure 3.6: Results for the NEI 120g 15 deg vs. 40 deg test. Both beds are subject to varying velocities and compression

There does not seem to be a head-loss dependence on the pressure washer nozzle angle used for NEI preparation because both the 80g and 120g fiber beds using 40deg and 15deg nozzles produced similar head-loss responses.

Repeatability Test

Another 40 gram test was performed for comparison against the initial test. The second test did not utilize 15 deg fiber, but only 40 deg fiber. The results of this second test are shown plotted against the results of the first 40 gram test's 40 deg data as seen below in Figure 3.7. The test indicates that error exists between the

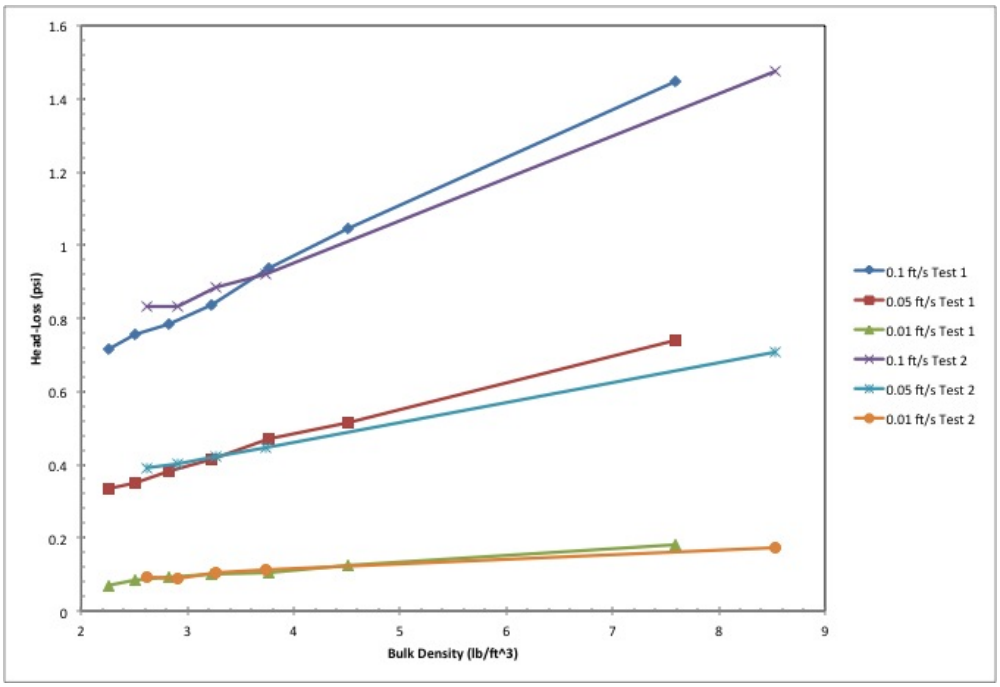

Figure 3.7: Results for the NEI 40g 40 deg Test 1 vs. Test 2.

two subsequent tests, especially at high velocity. This error is not of concern since previous results from 40g beds that indicate they behave more erratically than 80g and 120g beds. It is believed that if this duplicate test was performed for a 80g or 120g bed, that the error between subsequent tests would be minimal.

Discussion

The purpose of the varying nozzle test was to determine if varying the preparation technique for NEI with respect to the angle of the nozzle on the pressure washer would affect the hydraulic performance of the bed. The results indicate that for more massive beds, nozzle angle does not greatly affect the head-loss characteristics. It is hypothesized that the reason nozzle angle does not affect head-loss characteristics is because: one, the pressure washer used to make NEI fiber does not "cut" the fiber, it merely tears apart the grouping of the fiber strands by breaking the chemical bonds holding them together (from the fiberglass mat bonding agent), second, any bonding agent that remains after blasting from the pressure washer is likely dissolved when exposed to the flowing water of the SSFEL column. If both of these hypothesis' hold true, then it says that for fiberglass beds that have been adequately blasted, nozzle angle does not matter. The only results that contradict this hypothesis are the 40g beds, but, as explained earlier, the mass of these beds do not provide a large enough sample size or head loss to allow for bed homogeneity.

3.3 Mechanical Loading Response of an NEI Fiber Bed

It is desired to understand the mechanical response of an NEI fiberglass bed due to a load on the surface of the bed. This phenomena can represent chemical precipitate capturing on the surface of the bed during a LOCA scenario and experiencing drag from the flowing liquid, resulting in a force exerted by the precipitate on the surface of the fiberglass bed. This phenomena can be measured and characterized experimentally by understanding how bed compression is affected by loading force on the bed surface. The experiment involved loading a 120g fiberglass bed at 0.1

ft/s. The flow was then turned off, leaving the bed suspended in the stagnant fluid. Once the bed and fluid reached a steady-state an initial bed height was measured and recorded. Then, the compression screen was introduced into the system. The compression screen has its own mass and subsequently produced a force on the top of the bed when lowered onto it. The new bed height was measured after the screen was lowered. Next, weights were added one by one to the top of compression screen pole and steady-state bed heights were measured. The results from tests can be seen below in Figure 3.8.

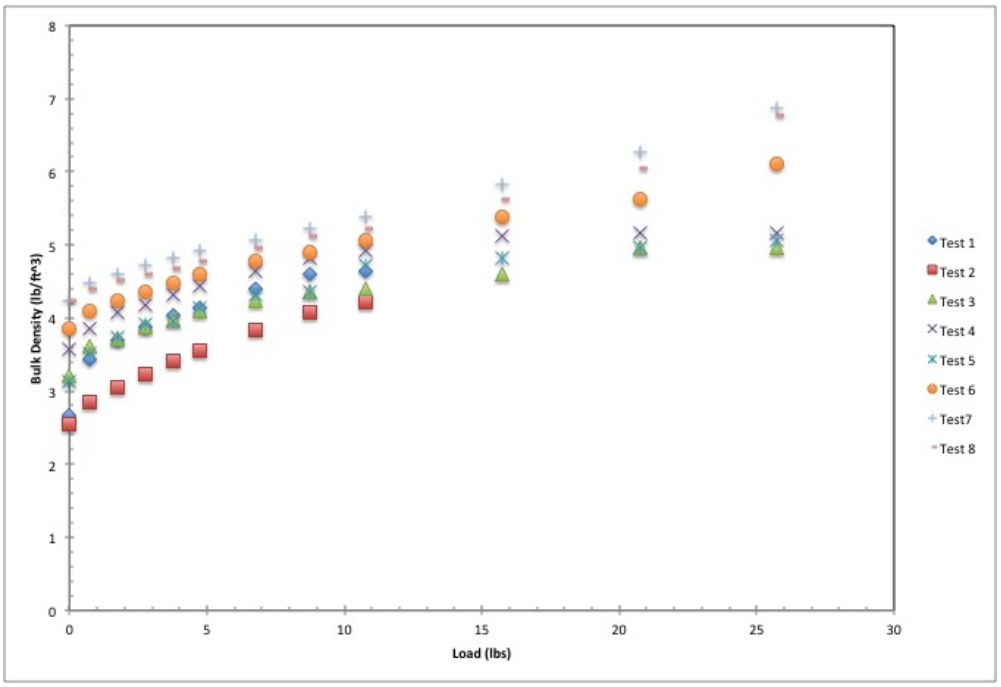

Figure 3.8: Mechanical Load Test on NEI 120g 40 deg Beds

The test results all agree that during the initial loading, the bulk density response is not linear as seen in Figure 3.9. This non-linear response is because the bed has yet to become evenly compacted. This means that the bulk density has not become uniform throughout the bed. Once the bed becomes uniform (determined from visual

inspection during experimentation), the bed responds linearly to loading. The beds for all the experiments do not agree with the density response loading value at higher loading values as seen in Figure 3.9. This is likely due to experimental error induced by the mechanism used to load the bed. As the bed was loaded, the compression screen pressed down on the top of the bed. Once about 10 lbs were loaded onto the

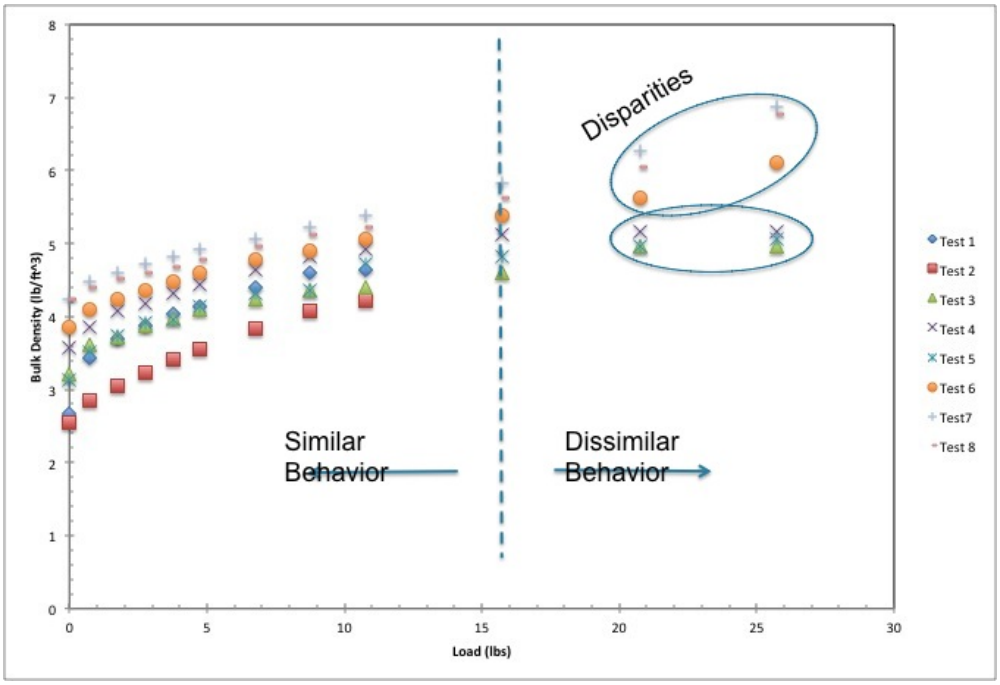

Figure 3.9: Mechanical Load Test on NEI 120g 40 deg Beds with comments

bed, the compression screen rod began to buckle ever so slightly. This would push the compression screen horizontally into the column wall.

The reason that Test's 3, 4, and 5 appear to level off at higher loads (20+ lbs) is because the compression screen was stuck to the wall and would not deflect downward onto the bed due to friction. This phenomena was noted and Test's 6,7, and 8 were performed differently than 3, 4, and 5 by slightly shaking the compression rod from the top in order to release the compression screen from the column wall. This allowed

the compression screen to continue deflecting the fiber bed surface. Test's 6, 7, an 8 were taken as the most representative and accurate results and are presented in Figure 3.10. Pressure was calculated from the applied load for Figure 3.10 for ease of future analysis. When only analyzing the results shown in Figure 3.10, it can be

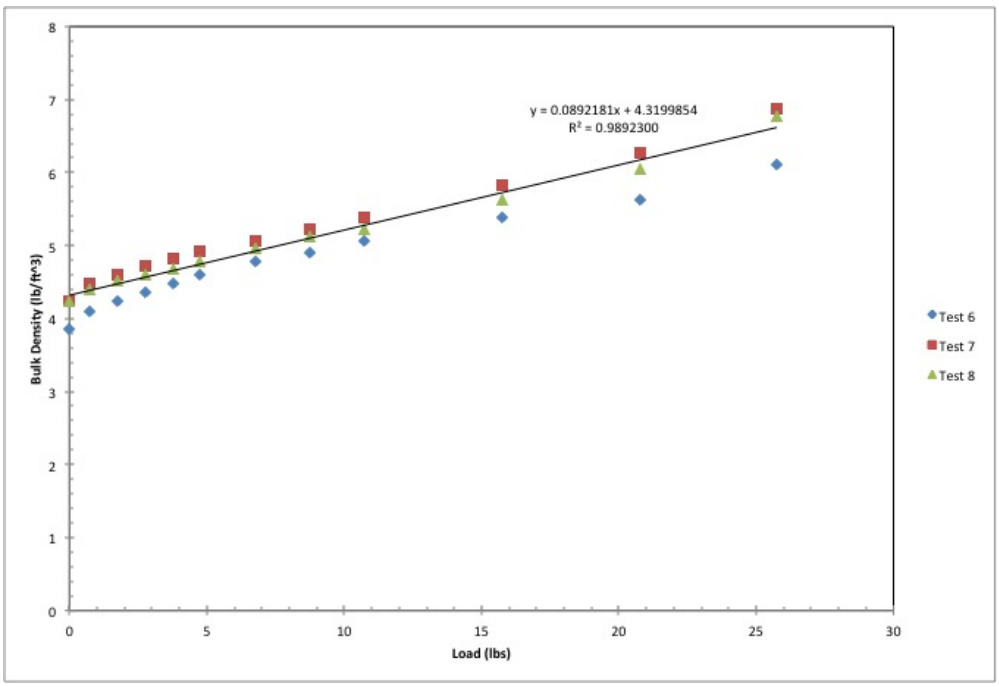

Figure 3.10: Mechanical Load Test on NEI 120g 40 deg Beds with Compression Rod Shaking to Allow for Proper Bed Deflection

seen that the compression of the bed behaves linearly at most pressures. The slope of the linear regression fit can be loosely described as a compression property of the fiberglass bed since it relates the density response of the bed to the load on the bed. The regression fit can help with the prediction of bulk density response of a bed dependent on the pressure on the surface of the bed. This information could prove quite useful to future fiberglass bed studies involving chemical precipitate.

3.4 Flow Induced Compression of an NEI Fiber Bed

Mechanically compressing a fiberglass bed does not represent how a bed will compress during a LOCA. Internal drag within the bed is the "loading" that a post-LOCA fiberglass bed will experience. This experiment aims to track bed characteristics as a function of fluid velocity, the primary factor leading to internal drag forces. Three tests were performed using NEI 80g 40 deg beds. Each bed was loaded into the manometer testing column at the lowest possible velocity (around 0.03 ft/s) and was allowed to settle to stead-state. Once at steady-state, the bed height and all the manometer tube readings were recorded. The velocity was then stepped up incrementally until max velocity was achieved, limited by the pump. At each increment, bed height and pressure readings were recorded. The results from the first bed (of three) can be seen below in Figure 3.11.

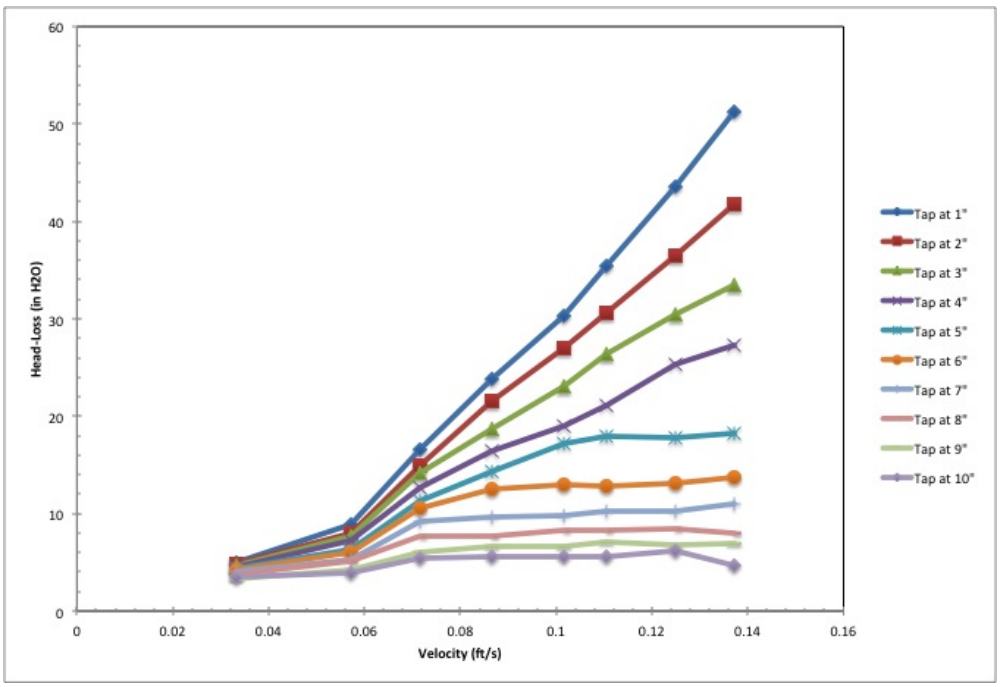

Figure 3.11: Flow Induced Head-Loss of an NEI 80g 40 deg Fiberglass Bed. Tap height corresponds to pressure reading at X inches above the bottom fiberglass bed screen.

The results indicate two things: first, measured pressure loss seems to be greatest at the bottom of the bed (tap at 1") and second, the relationship between measured pressure and flow rate appears to be dependent on location in the bed. One issue that arises with presenting the data as seen in Figure 3.11 is that the location of the tap is static within a dynamically distributed bed. Meaning that for the first velocity (lowest), the 10" pressure tap might be at 50 percent of the total bed height, but, once the velocity is increased and the bed height is now lower, the same tap may now be at 75 percent of the total bed height. The effect velocity has on bed height for this test can be seen in Figure 3.12.

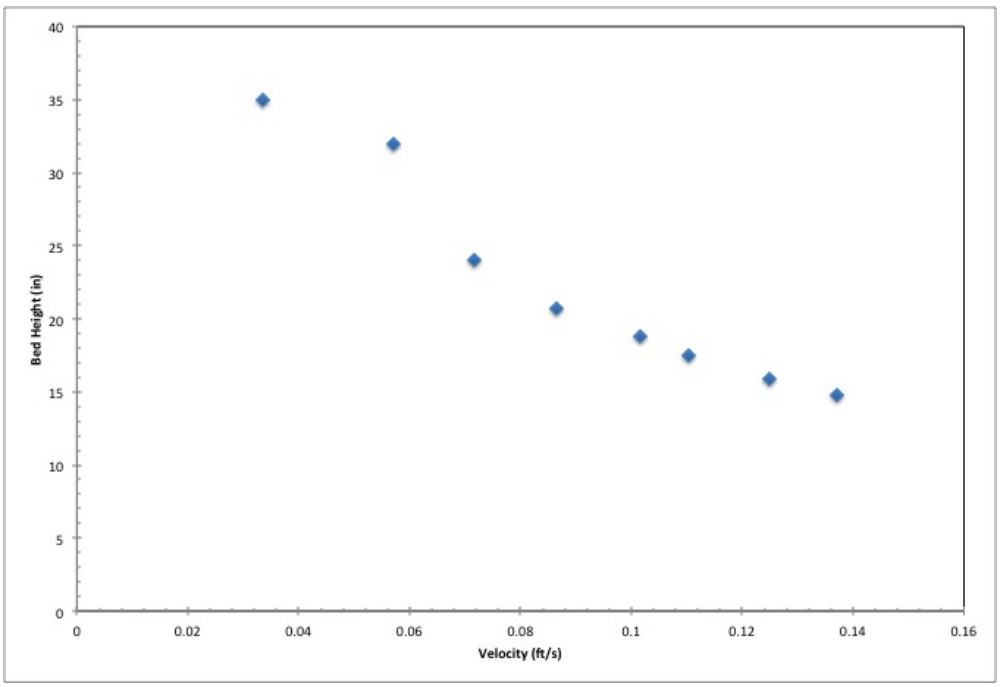

Figure 3.12: The bed height response of an NEI 80g 40 deg Fiberglass Bed to changing velocity

Because of this phenomena, the data was re-plotted using a value known as normalized location of the tap, which is simply defined as

$$RL = \frac{H_{tap}}{H_{bed}} \tag{3.2}$$

This allows for a better visual pressure distribution through the bed. The results of the third bed tested can be seen in this format in Figure 3.13. The third bed is shown because it demonstrates the clearest visual representation of experimental data even though the first and second tests produce similar results to Test 3. The results for Test 1 and Test 2 can be seen in the Appendix.

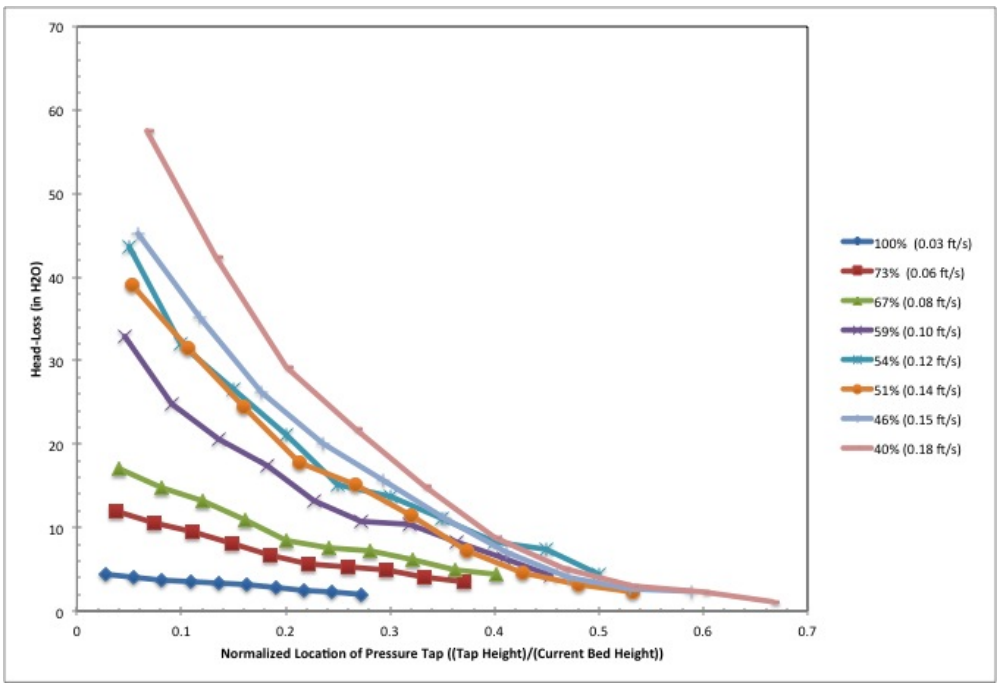

Figure 3.13: Flow Induced Head-Loss of an NEI 80g 40 deg Fiberglass Bed. Percentage in the legend corresponds to the percentage of original bed height and the velocity that induced that compression

This representation of the data allows one to see that at low velocities (0.03 ft/s), and a bed height of 36 inches, the pressure distribution through the bed is linear. As velocity is increased, the distribution of pressure through the bed becomes less and less linear. This behavior is likely due to the increased compression at the bottom of the bed from the fiber above it which can be represented by assuming non-uniform porosity (bulk density) throughout the bed. This relationship will be examined in more depth in the Analysis section.

3.5 Porosity Distribution due to Variable Velocity

Fiberglass bed porosity is not an easy parameter to measure since the porosity to be measured is dependent on the arrangement of the fiber matrix, not the fiber itself, and because fiberglass bed's are extremely porous (greater than 90%). To address some of the difficulties, an experiment was devised to track fiberglass bed porosity in sections of the bed as flow conditions were changed. An NEI 90g 40 deg fiberglass bed was made using six 15g sections of fiberglass. Each section of fiberglass was kept separate from the others. The samples can be seen in Figure 3.14.

Figure 3.14: 15g portions of NEI 40 deg fiberglass used in the Porosity Distribution Test

The first 15g sample was then loaded into the manometer testing column at a velocity of 0.09 ft/s. Once the first section of the fiberglass bed had reached a steady-state height, a mesh divider was added to the column and allowed to sit on top of the first fiberglass section. Once the mesh had settled, the second 15g section of fiber was loaded, followed by another mesh section. This process was repeated until the fiberglass bed was composed of six 15g sections of fiberglass separated by

5 mesh dividers. The loaded bed can be seen in Figure 3.15. The mesh dividers

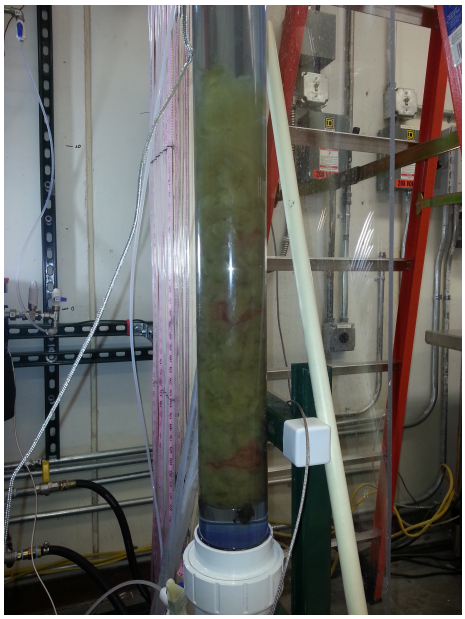

Figure 3.15: 15g portions of NEI 40 deg fiberglass separated by mesh dividers to compose a 90g bed.

do not appear to be completely horizontal in the loading, but during measurement, the same location on the divider was tracked. The test that ensued varied velocity and tracked the location of the 5 dividers. Since the mass of fiberglass between each divider was known and was constant (15g), the porosity between each divider can be calculated according to Equation 2.1. The results of the Porosity Test can be seen below in Figure 3.16. The results indicate that as flow rate is increased, all locations in the bed experience compression. It also indicates that locations nearest to the top of the bed experience the greatest compression as flow rate is increased. This is because there exists a non-uniform porosity distribution through the bed height when the bed is loaded. The porosity at the bottom of the bed is lowest and the top is highest. As porosity decreases it becomes harder and harder for bed compression to occur, hence why the high porosity upper section of the bed is compressed more

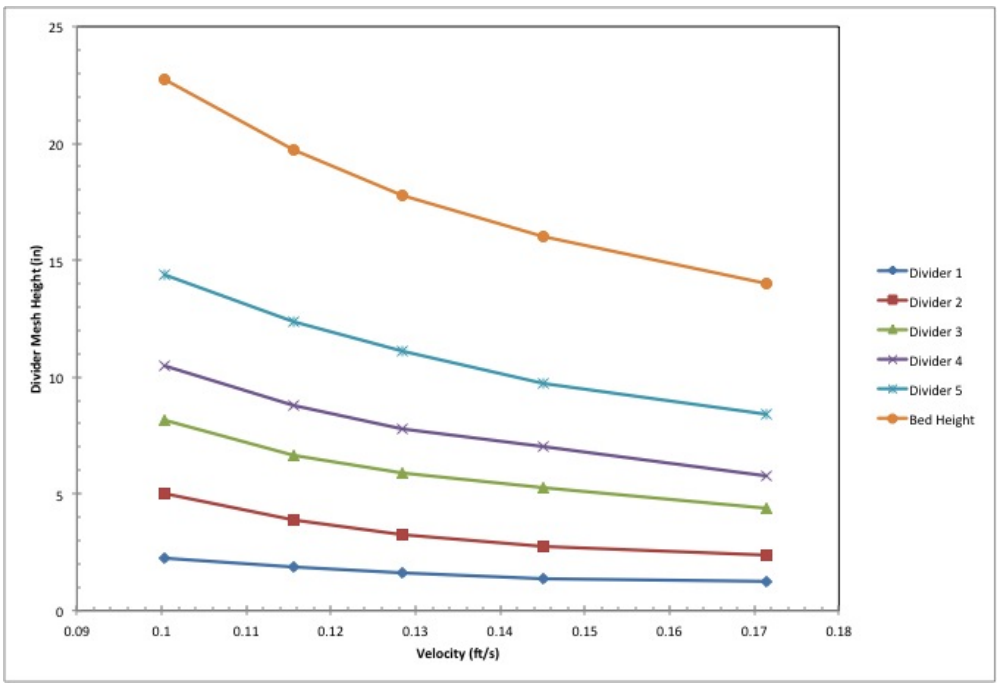

Figure 3.16: NEI 90g fiberglass bed used in Porosity Test tracking divider and bed height as a function of flow rate. Divider 1 corresponds to the divider closest to the bottom of the bed and divider 5 closest to the top of the bed.

than the bottom.

Porosity of each 15g section of the bed is shown with varying flow in Figure 3.17. The results are fitted with a linear regression model for each velocity step. The top most fit equation in Figure 3.17 corresponds to the lowest velocity (0.1 ft/s) and the bottom most fit equation corresponds to the greatest velocity (0.17 ft/s). Each velocity line does seem to have a data point that behaves differently than the others at the 0.2 to 0.3 normalized divider location. Departure from linear behavior is likely due to heterogeneity in the bed and uneven tilt of the mesh dividers. Sometimes clumps of fiber can get stuck on the column wall and not behave like fiber that is not still bonded by remnant binder chemicals, this, and the behavior of the mesh itself, are the most likely explanations for imperfect bed behavior.

The porosity test is a very important test because it allows for a non-uniform distribution of porosity through a fiberglass bed to be characterized. Figure 3.17 shows that porosity is both spatially and velocity dependent in a fiberglass bed. The linear regression models gained from Figure 3.17 will be vital in developing a model for porosity to be developed in the analysis section.

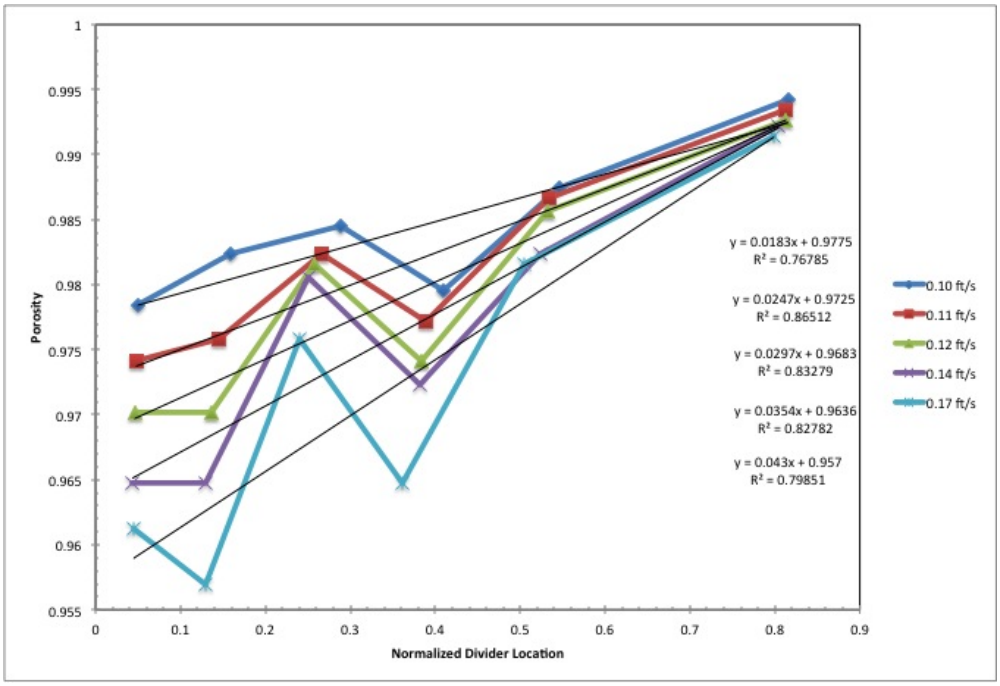

Figure 3.17: NEI 90g fiberglass bed used in Porosity Test tracking porosity as a function of flow rate and location in the bed.

Chapter 4

Analysis and Ergun Equation Formulation

The goal of the experiments conducted is to develop a model for predicting head-loss across a fiberglass bed dependent on its mass and flow conditions. Experiments have allowed for an understanding of how porosity is affected by flow and location, how bulk bed compression affects pressure responses, how mechanical compression affects pressure response, and how NEI preparation technique affects pressure response. Below is outlined how all of these experiments were interpreted together to develop a unified model.

4.1 Porosity Relation

It was experimentally observed that porosity is a function of two things, packing of a fiber bed and location in the fiber bed. The packing of the fiber bed is a function of both mass of fiberglass and the flow velocity. The packing term in porosity will now be known as linear density. The linear density used is the average linear density of

the entire bed. Linear density is the mass of fiber per height of the bed. It is defined as:

$$LD = \frac{m_{fiber}}{H_{bed}} \tag{4.1}$$

Utilizing the linear density (LD) along with bed relative location, Equation 3.2, porosity (ϵ) can now be a function of linear density and relative location (RL) or

$$\epsilon = \epsilon(LD, RL) \tag{4.2}$$

The first step to solving for porosity in terms of linear density and relative location is plotting porosity as a function of linear density and relative location by utilizing the linear regression models obtained from Figure 3.17 (outlined below in Equation's 4.3, 4.4, 4.5, 4.6, and 4.7) and calculating the corresponding linear densities at each velocity the fit was attained from.

$$Velocity = 0.1 ft/s, \epsilon = 0.0183 * RL + 0.9775 \tag{4.3}$$

$$Velocity = 0.11 ft/s, \epsilon = 0.0247 * RL + 0.9725 \tag{4.4}$$

$$Velocity = 0.12 ft/s, \epsilon = 0.0297 * RL + 0.9683 \tag{4.5}$$

$$Velocity = 0.14 ft/s, \epsilon = 0.0354 * RL + 0.9636 \tag{4.6}$$

$$Velocity = 0.17 ft/s, \epsilon = 0.043 * RL + 0.957 \tag{4.7}$$

The results can be seen graphically in Figure 4.1. The experimental results were then fit to a continuous polynomial model utilizing a quadratic term for linear density (since linear density is, in itself a function of two independent variables) and a linear term for relative location. The results of the fitted surface can be seen in Figure 4.2.

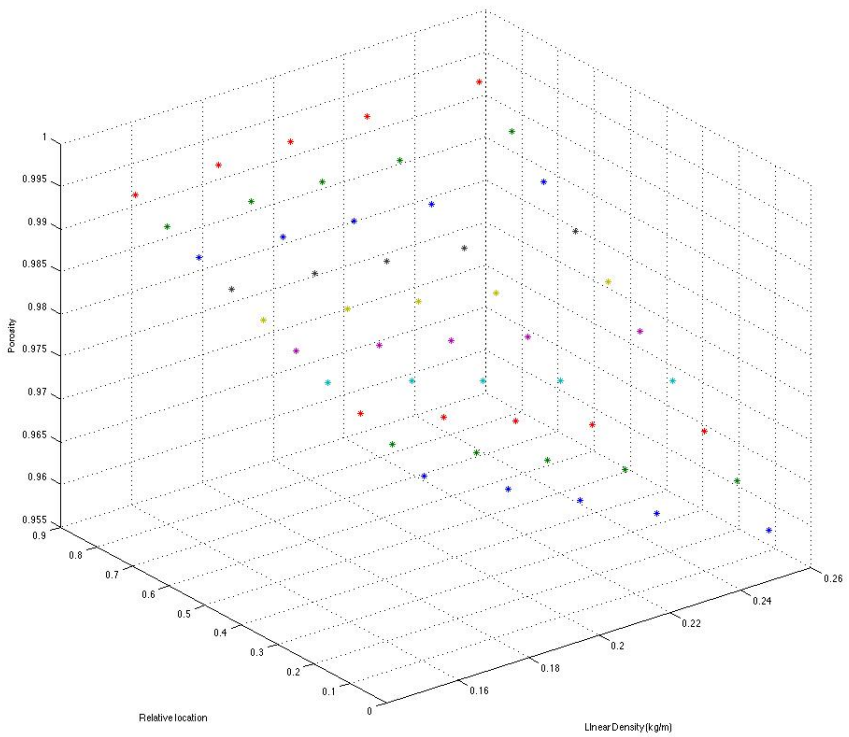

Figure 4.1: Porsity plotted as a function of linear density and relative location utilizing Equation's 4.3, 4.4, 4.5, 4.6, and 4.7

The resulting surface fit yields the following fit equation

$$\epsilon(RL, LD) = p00 + p10 * RL + p01 * LD + p11 * RL * LD + p02 * LD^2 \quad (4.8)$$

The parameters for the fit are listed in Table 4.1 The final equation for porosity as a function of Relative Location and Linear Density can be seen in Equation 4.9

$$\epsilon(RL, LD) = 1.007 - 0.02096RL - 0.182LD + 0.2535RL * LD - 0.07019LD^2 (4.9)$$

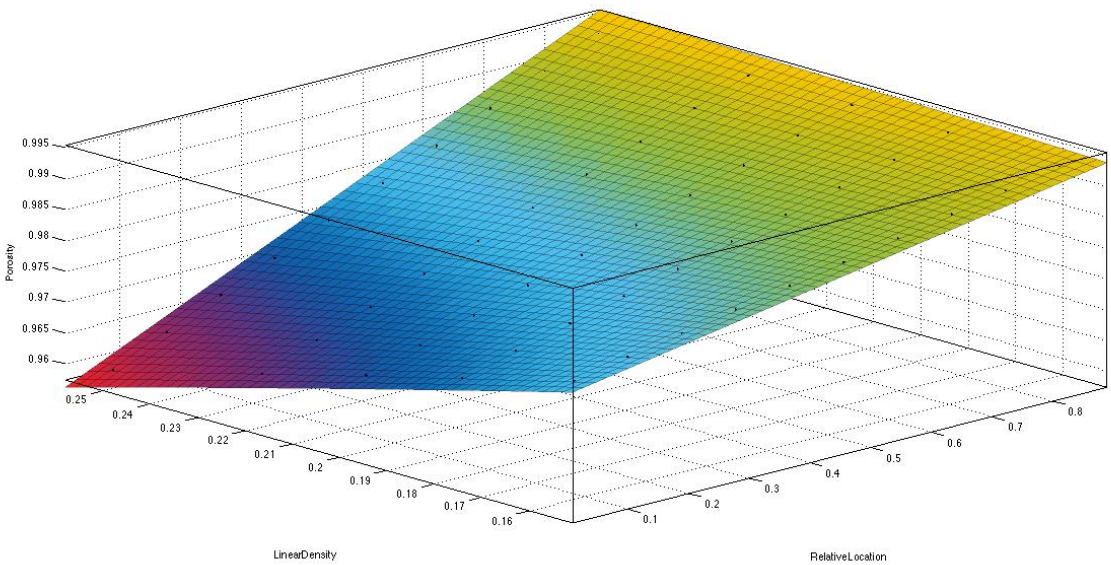

Figure 4.2: Porosity surface fitted to linear density and relative location using Matlab polyfit tool. Linear Density in kg/m

Table 4.1: Porosity Fit Parameters, $R^2 = 1$

Parameter	Value	95% Conf. Lower	95% Conf. Upper
p00	1.007	1.007	1.008
p10	-0.02096	-0.02132	-0.0206
p01	-0.182	-0.1881	-0.1756
p11	0.2535	0.2518	0.2553
p02	-0.07019	-0.08498	-0.0554

4.2 Linear Density Relation

Linear density is function of velocity and mass of the fiberglass bed. In order to properly represent bed mass outside of the SSFEL setup, bed mass will be fit utilizing specific bed mass, defined by Equation 4.10

$$m_{sp} = m_{fiber}/SA_{screen} \tag{4.10}$$

where,
m_{sp} *is the specific mass of the bed*
m_{fiber} *is the mass of the entire fiberglass bed*
SA_{screen} *is the surface area of the bottom screen (experiment) or sump screens (nuclear plant)*

The flow induced compression series of tests along with the porosity distribution test, provide the data necessary to develop a relationship for linear density as a function of specific bed mass and velocity. Below in Figure 4.3, the bed average linear density is plotted as a function of specific bed mass and velocity for the three flow induced compression tests and the one bed porosity test. Next, the data was fitted to a polynomial with velocity and specific bed mass as linear terms. The plotted fit can be seen below in Figure 4.4. The equation of fit for Figure 4.4 takes the form

$$LD(m_{sp}, v) = p00 + p10 m_{sp} + p01 v \tag{4.11}$$

with fit parameters described in Table 4.2. The final model for Linear Density (kg/m) as a function of Specific Bed Mass (kg/m^2) and Velocity (m/s) is

$$LD(m_{sp}, v) = 0.01806 + 0.002059 m_{sp} + 1.093 v \tag{4.12}$$

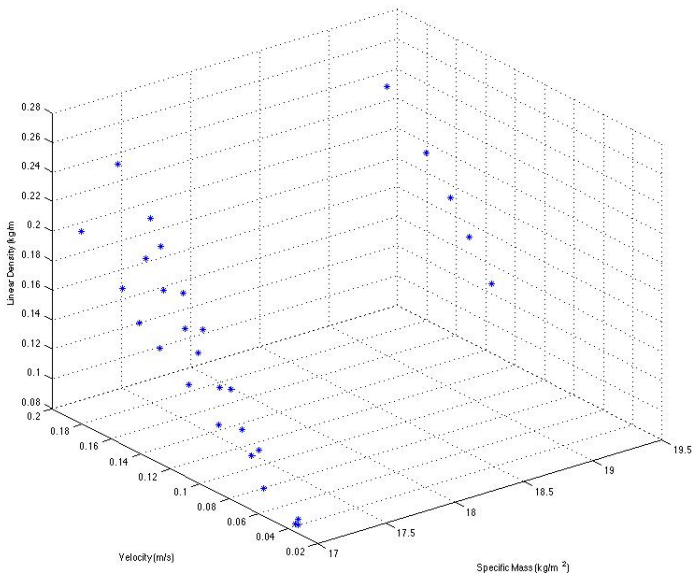

Figure 4.3: Linear Density plotted as a function of velocity and specific bed mass

Table 4.2: Linear Density Fit Parameters, $R^2 = 0.7927$

Parameter	Value	95% Conf. Lower	95% Conf. Upper
p00	0.01806	-0.1817	0.2178
p10	0.002059	-0.009783	0.0139
p01	1.093	0.8539	1.332

4.3 Ergun Constant Fitting and the HFH Correlation

Now that a relationship for porosity as a function of specific bed mass, velocity, and relative location has been found, the Ergun Constant, K, from Equation 1.4, can be solved for. Utilizing data gathered from the flow induced compression test, Equation's 4.9 and 4.12, assuming "d" in Equation 1.4 is 7.1 μm [15], and solving

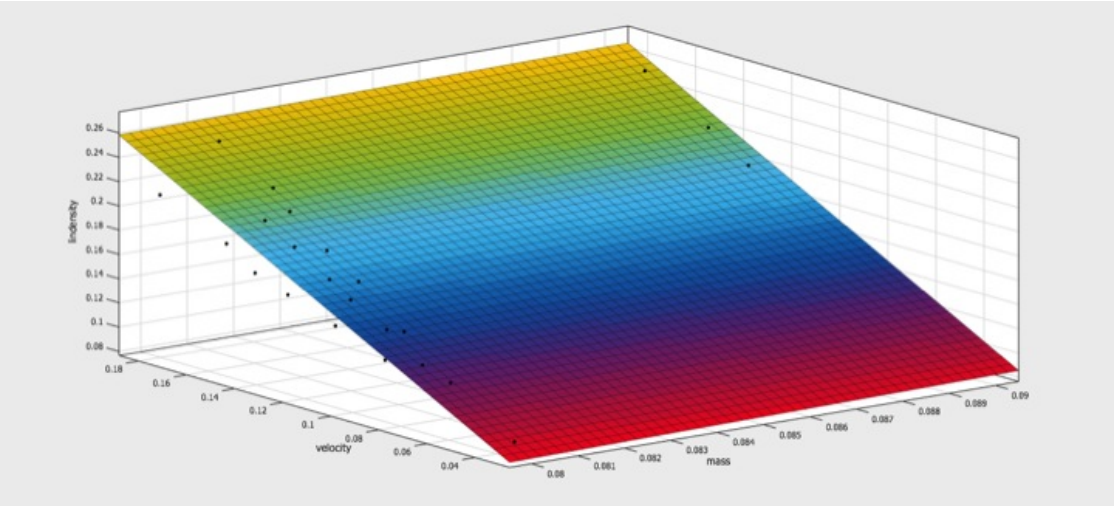

Figure 4.4: Linear Density (kg/m) plotted as a function of velocity (m/s) and specific bed mass (kg/m2)

for "K" yields the Ergun Constant. In doing so, 240 individual values of K are obtained from the flow induced compression test data. Figure 4.5 shows "K" plotted against porosity. The data appears to be more consistent at lower porosities. This confirms what was previously hypothesized that bed mechanics are more predictable when the bed is more compressed (lower porosity). This is due to increased homogeneity within the bed itself. The average "K" value was found to be 38.8 with a standard deviation of ± 21.7. Utilizing the newly calculated "K", a correlation that relates head-loss across a fiberglass bed as only a function of mass of fiber, sump screen cross-sectional area, approach velocity, fiber diameter, and viscosity can be formulated. This correlation will be named the Hammond-Fiberglass-Head-Loss correlation (HFH). The HFH correlation treats a fiberglass bed as a highly compressible media (the fiber matrix) with a non-uniform, linear in this case, porosity as a function of depth in the bed. The correlation is a derivative of the Ergun Equation with two distinct differences. First, the second "kinetic" term of the Ergun equation has been excluded in the HFH correlation because inertial effects are not significant at

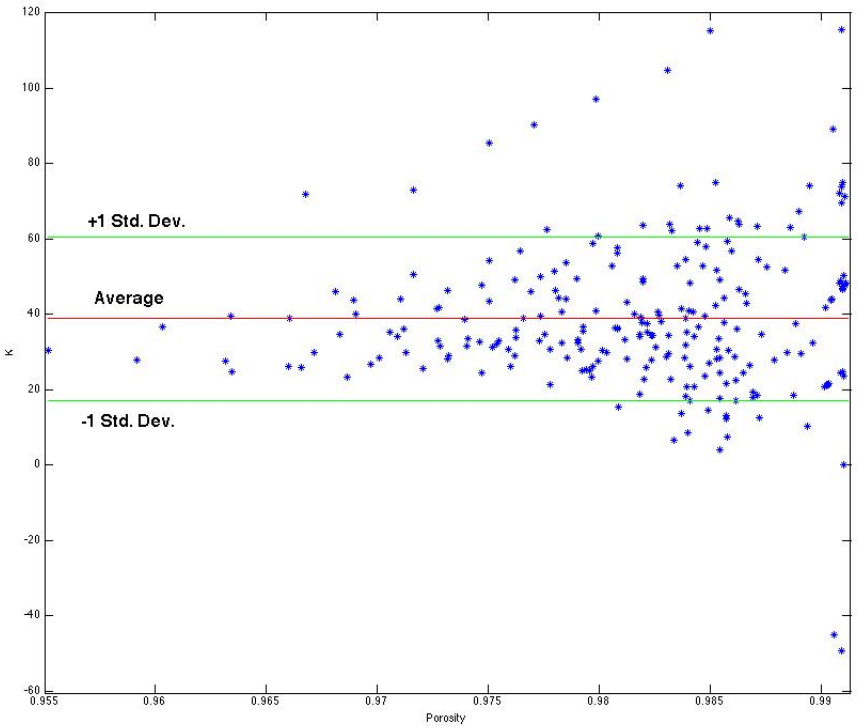

Figure 4.5: "K" plotted against porosity.

the flow regime of interest (Particle $Re < 1$). Second, Ergun assumes incompressibility (constant porosity through depth of media), the HFH correlation assumes the bed is compressible and experiences non-uniform (constant) porosity. It is worth noting that "L", the media thickness in the Ergun equation, has been replaced by $\frac{m}{\rho_L}$, which is the fiberglass bed thickness. The HFH correlation in differential form (Equation 4.15) can be seen below. Note linear density is now denoted by ρ_L and relative location is now denoted by z_r.

$$\rho_{L,avg}(m_{sp}, v) = 0.01806 + 0.002059 m_{sp} + 1.093 v \tag{4.13}$$

$$\epsilon(z_r, \rho_L) = 1.007 - 0.02096 z_r - 0.182 \rho_{L,avg} + 0.2535 z_r \rho_{L,avg} - 0.07019 \rho_{L,avg}^2 \quad (4.14)$$

$$dP = 38.8 \frac{m}{\rho_{L,avg}} \frac{(1 - \epsilon(z_r, \rho_{L,avg}))^2}{\epsilon(z_r, \rho_{L,avg})^3} \frac{\mu U}{d^2} dz_r \quad (4.15)$$

All units are metric $\Big[dP(Pa), \rho_{L,avg}(\frac{kg}{m}), m_{sp}(\frac{kg}{m^2}), \mu(Pa-s), U(\frac{m}{s}), d(m), m(kg)\Big]$

The total pressure drop across an arbitrary relative section of the bed can be solved for by integrating the right side of Equation 4.15 by dz_r (relative location) and the left side by dP. The resulting equation can be seen in Equation 4.16. dP will be the head-loss between any two relative points in the bed (z_{r1} and z_{r2}). z_{r1} is the point closest to the screen and z_{r2} is the point closest to the bed surface.

$$P = 38.8 \frac{m}{\rho_{L,avg}} \frac{\mu U}{d^2} \int_{z_{r1}}^{z_{r2}} \frac{(1 - \epsilon(z_r, \rho_{L,avg}))^2}{\epsilon(z_r, \rho_{L,avg})^3} dz_r \quad (4.16)$$

Finally, the total head-loss across a fiberglass bed can be attained by setting $z_{r1} = 0$ (bottom of the bed) and $z_{r2} = 1$ (top of the bed) seen in Equation 4.17.

$$P = 38.8 \frac{m}{\rho_{L,avg}} \frac{\mu U}{d^2} \int_{0}^{1} \frac{(1 - \epsilon(z_r, \rho_{L,avg}))^2}{\epsilon(z_r, \rho_{L,avg})^3} dz_r \quad (4.17)$$

4.4 Confirmation of HFH Correlation

The HFH correlation was compared to measured experimental data from the Flow Induced Compression Test. The first comparison was for the predicted linear density ($\rho_{L,avg}$) as a function of the fiberglass specific bed mass and flow velocity. The results of the comparison can be seen in Figure 4.6; The predicted linear density does appear to represent the data well. The difference in experimental data and the fit is due to heterogeneous fiber deposition in the bed. The second comparison is of the actual head-loss through the fiberglass bed during the Flow Induced Compression test and the HFH predicted head-loss. These results can be seen in Figure 4.7. As Figure 4.7

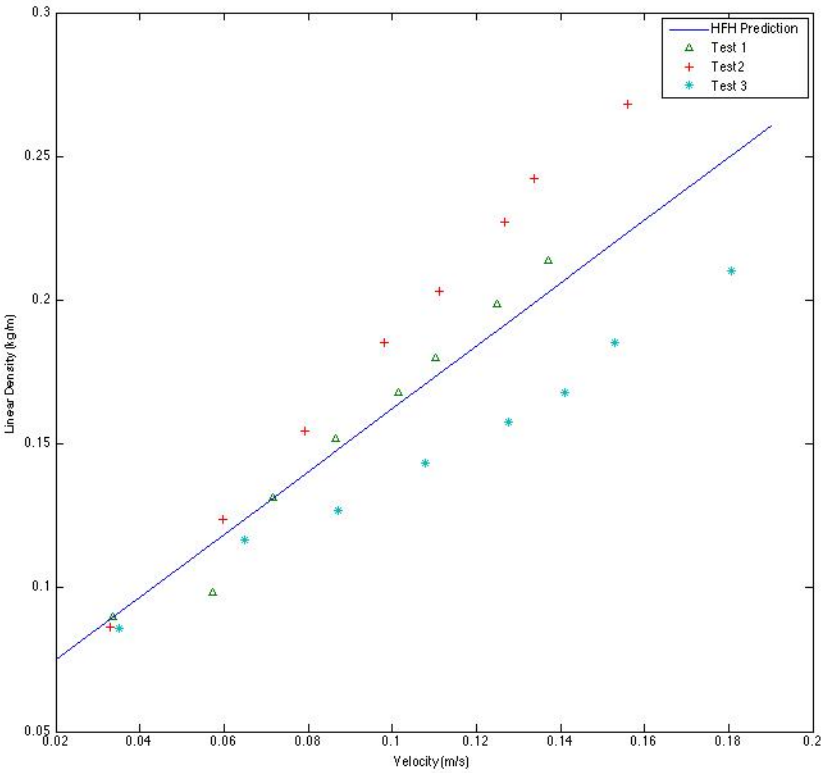

Figure 4.6: HFH Predicted Linear Density compared to the Flow Induced Compression Test Results for a 0.083 kg fiberglass bed

shows, the HFH correlation does a good job predicting the head-loss for the plotted experiments. It does overestimate head-loss slightly, but is not too concerning since the application of the HFH is nuclear accident scenarios when overestimation of head-losses is a conservative estimate.

It is also important to compare experimental data with the HFH correlation, the 6224 correlation [10], and the Ergun equation. Figure 4.8 shows this comparison. It can be seen that the HFH correlation fits the experimental head-loss data much better than the 6224 correlation which greatly underestimates head-loss at higher

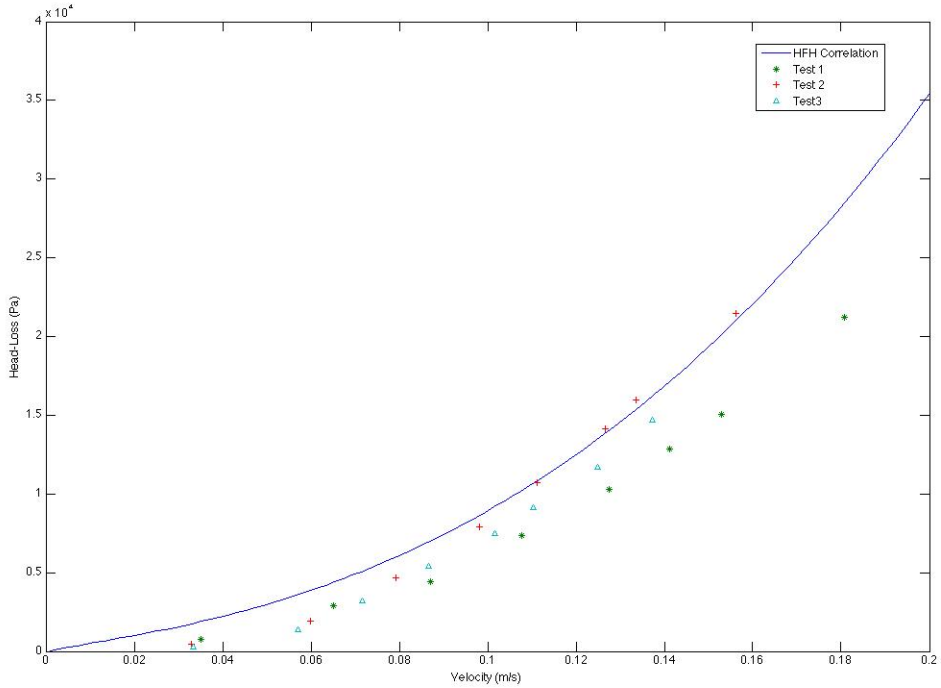

Figure 4.7: HFH Predicted Head-Loss Across the Entire Fiberglass Bed Compared to the Flow Induced Compression Test Results. The bed mass used is 0.083 kg

velocities. The Ergun equation over predicts head-loss at all velocities. It must be noted that the 6224 correlation and the Ergun Equation do not contain a metric for predicting porosity as a function of velocity, as such, the HFH correlation porosity prediction technique, Equation 4.9, was used to predict the bulk porosity (uniform throughout the bed) as a function of velocity, for input into the 6224 correlation and Ergun Equation.

It would also be beneficial to have a visual representation of how the HFH predicts head-loss as a function of both bed mass and velocity. This behavior, along with predicted bed height, can be seen in Figure 4.9. Figure 4.9 provides a visual representation of a tool (HFH) to understand how fiberglass bed characteristics are

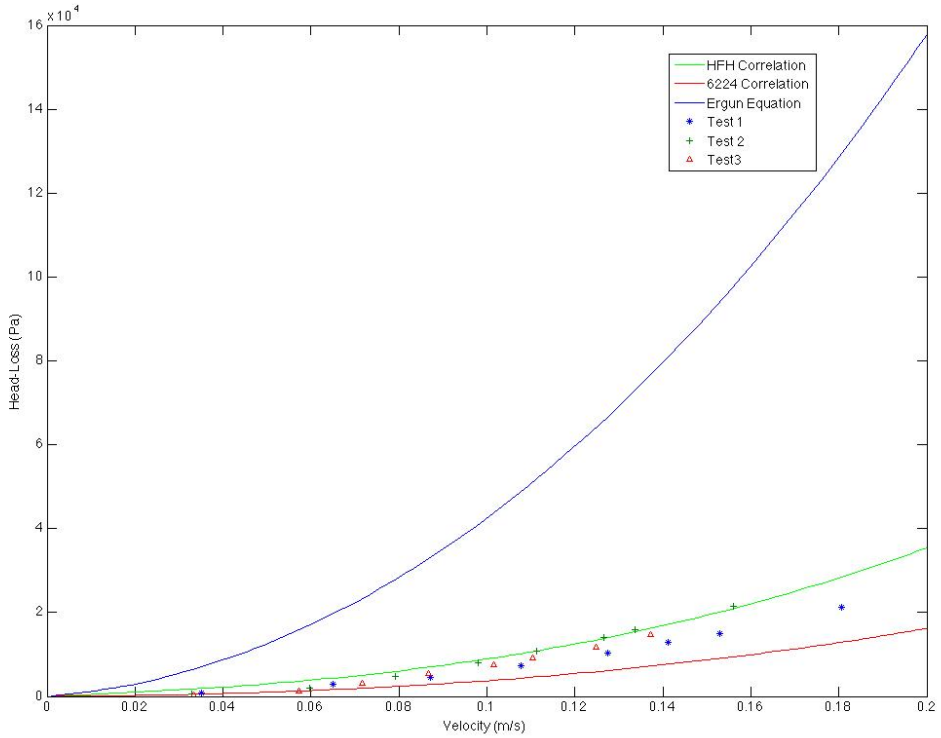

Figure 4.8: HFH Predicted Head-Loss Across the Entire Fiberglass Bed Compared to the 6224 Correlation, the Ergun Equation, and the Flow Induced Compression Test Results. The Bed Mass Used is 0.083 kg.

affected by multiple variables. This information will be very useful in predicting head-loss in post-LOCA fiberglass beds.

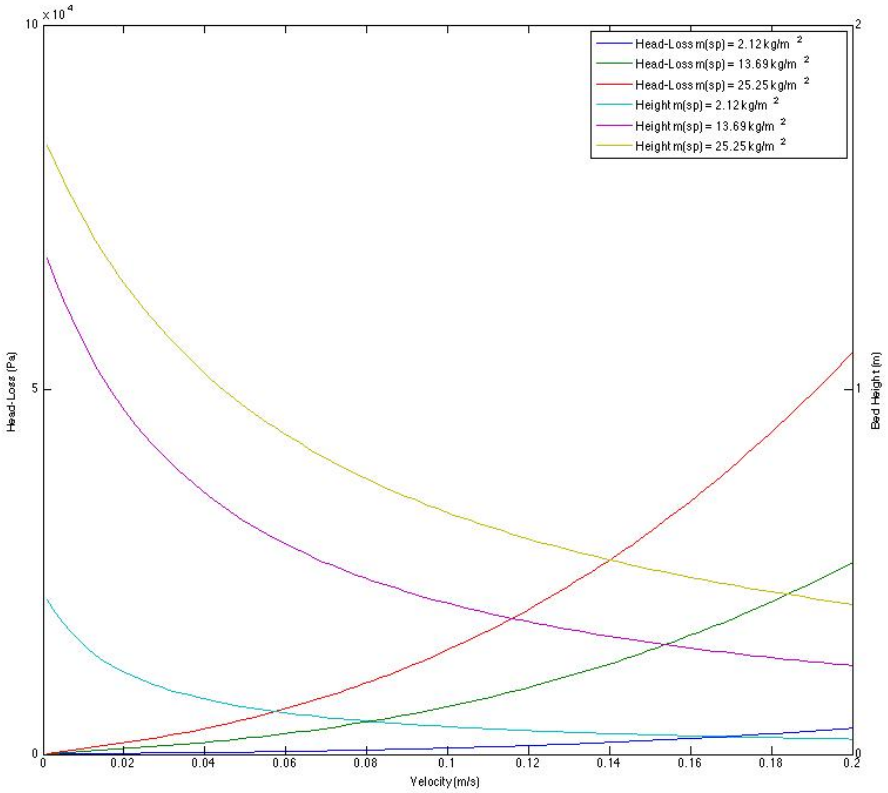

Figure 4.9: HFH Predicted Head-Loss Across and Total Bed Height for Varying Specific Bed Mass and Velocity

4.5 Error Analysis

A discussion of error is always necessary when completing experimental work. The research performed is not an exception to the rule. The most important values (correlations) obtained are linear density, porosity, and the K constant. Each of these values or correlations is composed of both systematic and random error. Each of these values also contributes to error in the HFH correlation. It is useful to understand the systematic error for each of these values or correlations.

4.5.1 Error within the Linear Density Correlation

The linear density correlation, Equation 4.12, is a function of both specific bed mass and velocity. Velocity is measured by the Omega flow meter described in the Instrumentation section. This flow meter experiences an average error of ±1.5% [17]. The scale used to weigh the fiber has an error of approximately ±0.05% at weights used during testing. The error in the screen surface area is not known. This leaves velocity with an error of ±0.5% and specific mass with ±0.05%. Since these values are added together in the linear density correlation the error on the correlation is determined to be

$\rho_{L,avg}(error) = \pm 0.5\%$

4.5.2 Error within the Porosity Correlation

The porosity correlation, Equation 4.9, is a function of relative location and linear density. The greatest error from the measurement device (resolution of the measurement) used to measure beds will occur while measuring the shortest beds. The measurement device can measure to the 1/8", this leads to an error of ±0.11% for the shortest beds. The linear density error was already determined to be ±0.5%. Porosity is a function of linear density squared, linear density multiplied by relative location, linear density, and relative location. Using compounding error formulations, the error on porosity measurements is

$\epsilon(error) = \pm 1.02\%$

4.5.3 Error within the K Constant

The K Constant is composed of manometer tube pressure readings, velocity readings, bed height readings, and bed mass readings. Velocity, bed height, and bed mas

reading errors are already understood. Manometer tube pressure reading resolution is 1/8", at the lowest readings this gives a maximum error of approximately ±4%. The K constant is a product of the Ergun equation which involves porosity, pressure, bed height, and velocity. The K constant will then have an error of approximately
$K(error) = \pm 4.32\%$

4.5.4 Error on HFH Correlation

The HFH correlation is composed of porosity, velocity, bed height, and the K constant. When all of these errors are combined, according to the correlation, the error becomes
$HFH(error) = \pm 6.1\%$

Chapter 5

Closing Remarks

The goal of experimentation was to develop an equation, based on the Ergun Porous Flow Head-Loss Equation, to predict head-loss through a post-LOCA fiberglass bed as a function of system conditions (velocity) and fiber bed characteristics (mass). The goal was achieved as a correlation to predict head-loss was generated that is only a function of specific bed mass and velocity $P_{hl} = P(m_{sp}, v)$ for head-loss across the entire bed and a function of $P_{hl} = P(m_{sp}, v, z_r)$ for head-loss across sections of the bed. The HFH correlation will prove crucial to future GSI-191 work involving accident modeling. The correlation allows one to specify a mass of fiber and an approach velocity for sump screens and generate bed height, bed porosity, and head-loss data. To the knowledge of the author, bed height and bed porosity predictions have never been established for fiberglass beds.

There is plenty of experimentation still to be done for modeling post-LOCA fiberglass beds. The interaction of fiberglass beds and chemical precipitate is one example. This research established a symbolic compression response for fiberglass beds subject to a surface loading seen in Figure 3.10 which represents chemical precipitate captured on the surface of the fiberglass bed. This effect can be coupled

with the HFH correlation to predict linear density of the bed composed of two components, the flow induced density throughout the entirety of the bed and the density component from a load on the surface of the bed. Another area of future research may lie within understanding the blenderized fiberglass bed. Research has been done previously to characterized a blenderized bed [9], but an attempt at understanding the porosity-depth relationship has not been attempted.

The HFH correlation is the first step in understanding a fiberglass bed both thoroughly and fundamentally. Some instances of previous work simply fitted a constant (Ergun) to a porous flow equation and ignored the fact that fiberglass beds are not uniform porosity. The fiberglass bed is a highly porous and highly compressible media, making it a very unique flow structure. The HFH correlation addresses the issue of non-uniform porosity and provides an avenue to predict bed characteristics using velocity and mass. In conclusion, the developed correlation satisfies and exceeds the goals set out by this thesis and significantly contributes to the fundamental understanding of fiberglass bed mechanics.

References

[1] B.C. Letellier, *A selection of problems and results in Theoretical Treatment of Pressure Gradients in One-Dimensional, Inhomogeneous, Compressible Media*, No. LA-UR-13-20761, Los Alamos National Laboratory (LANL), 2013.

[2] C.W. Enderlin, B.E Wells, et al., *Experimental Measurements of Pressure Drop Across Sump Screen Debris Beds in Support of Generic Safety Issue 191*, Pacific Northwest National Laboratory, 2007.

[3] D.V. Rao, B.C. Letellier,et al., *GSI-191 Technical Assessment: Summary and Analysis of U.S. Pressurized Water Reactor Industry Survey Responses and Responses to GL 97-04*, U.S. Nuclear Regulatory Commission, NUREG/CR-6762, Vol. **2**, 2002.

[4] J. Leavitt, K. Howe, *T2 LBLOCA Test Report*, CHLE-014, University of New Mexico, 2012.

[5] A.K. Maji, D.V. Rao, B.C. Letellier, *Transport Characteristics of Selected PWR LOCA Generated Debris*, LA-UR-00-4998, NRC Water Reactor Safety Meeting, 2000.

[6] J. Leavitt, K. Howe, *T1 MBLOCA Test Report*, CHLE-012, University of New Mexico, 2012.

[7] S. Egun, Chem Process Eng. London 48, 89, 1952.

[8] N.S. Cheng, *Wall Effect on Pressure Drop in Packed Beds*, Powder Technology, 210(3), 261-266, 2011.

[9] C.W. Enderlin, B.E. Wells, M. White, F. Nigl,D.R. Rector, T.J. Peters, A.D. Guzman, *Experimental Measurements of Pressure Drop Across Sump Screen Debris Beds in Support of Generic Safety Issue 191*, PNNL-16313, Pacific Northwest National Laboratory, 2007.

[10] G. Zigler, J. Brideau, D.V. Rao, C.J. Shaffer, F. Souto, W. Thomas, *Parametric Study of the Potential for BWR ECCS Strainer Blockage Due to LOCA Generated Debris*, NUREG/CR-6224, U.S. Nuclear Regulatory Commission, 1995.

[11] Nuclear Energy Institue (NEI), *ZOI Fibrous Debris Preparation: Processing, Storage, and Handling, Revision 1*, January 2012.

[12] J. Leavitt, K. Howe, *Determination of the initial pool chemistry for the CHLE test*, CHLE-005, University of New Mexico, 2012.

[13] P.C. Carman,*Fluid Flow Through Granular Beds*,Transactions, Institution of Chemical Engineers, London,15: 150-166, 1937.

[14] PCI Engineering Systems Group, *NUKON Thermal Insulation System*, NUKON Brochure.

[15] Nuclear Engineering Institue, *Appendix V, Confirmatory Head-Loss Analyses*, work for NRC CR-6224, ML043280013, 2004.

[16] PCI Engineering Systems Group, *NUKON Thermal Insulation System MSDS*, NUKON Brochure.

[17] Omega Engineering, *FMG-3000 SERIES Blind Version Magmeter*, omega.com.

Appendices

Appendix A

Experimental Results

A.1 NEI Varying Nozzles Results

The results from the nozzle test can be seen below.

Bed	Spray Angle (°)	Mass (g)	Height Down (in)	Height Up (in)	Flow Rate Down (gpm)	Flow Rate Up (gpm)	DP Down (psi)	DP Up (psi)
1	0	40.480	8.750	8.500	1.940	1.950	0.717	0.720
1	0	40.480	8.750	9.000	1.000	0.990	0.364	0.356
1	0	40.480	9.000		0.540		0.204	
2	15	40.240	8.750		1.880		0.689	
3	25	40.300	8.250		1.860		0.750	
4	40	40.360	8.750	8.500	1.910	1.900	0.757	0.758
4	40	40.360	8.750	8.750	0.990	0.990	0.391	0.378
4	40	40.360	9.000		0.530		0.208	

A.2 NEI Compression and Velocity Variation Results

The results from the NEI Compression and Velocity Variation test can be seen below.

	Initial Height (in)	9.25												
Nozzle (deg)	Mass (g)	Compression (%)	Height (in)	Porosity	Bulk Density (lb_fiber/in^3)	Flow Rate 0.1 ft/s (gpm)	Flow Rate 0.05 ft/s (gpm)	Flow Rate 0.01 ft/s (gpm)	Velocity 1 (ft/s)	Velocity 2 (ft/s)	Velocity 3 (ft/s)	DP 1 (psi)	DP 2 (ft/s)	DP 3 (ft/s)
40	40.03	0	9.25	0.9855343	0.001307548	2.3	1.13	0.21	0.101131	0.0496861	0.0092337	0.7158	0.3345	0.07
40	40.03	10	8.325	0.983927	0.001452832	2.31	1.13	0.24	0.1015707	0.0496861	0.0105528	0.756	0.3503	0.085
40	40.03	20	7.4	0.9819178	0.001634436	2.3	1.15	0.24	0.101131	0.0505655	0.0105528	0.7857	0.3832	0.0907
40	40.03	30	6.475	0.9793347	0.001867926	2.29	1.15	0.25	0.1006913	0.0505655	0.0109925	0.8379	0.4123	0.1023
40	40.03	40	5.55	0.9758905	0.002179247	2.3	1.17	0.23	0.101131	0.0514449	0.0101131	0.935	0.4697	0.1056
40	40.03	50	4.625	0.9710686	0.002615097	2.31	1.16	0.25	0.1015707	0.0510052	0.0109925	1.0452	0.5153	0.1247
40	40.03	70.27	2.75	0.951343	0.004398118	2.31	1.15	0.25	0.1015707	0.0505655	0.0109925	1.4461	0.74093	0.1825
	Initial Height (in)	11.5												
Nozzle (deg)	Mass (g)	Compression (%)	Height (in)	Porosity	Bulk Density (lb_fiber/in^3)	Flow Rate 0.1 ft/s (gpm)	Flow Rate 0.05 ft/s (gpm)	Flow Rate 0.01 ft/s (gpm)	Velocity 1 (ft/s)	Velocity 2 (ft/s)	Velocity 3 (ft/s)	DP 1 (psi)	DP 2 (ft/s)	DP 3 (ft/s)
40	80.05	0	11.5	0.976732	0.00210185	2.3	1.16	0.23	0.101131	0.0510052	0.0101131	2.142	1.0513	0.2438
40	80.05	10	10.35	0.9741466	0.002336872	2.31	1.15	0.21	0.1015707	0.0505655	0.0092337	2.19132	1.0767	0.2283
40	80.05	20	9.2	0.9709149	0.002628981	2.3	1.15	0.23	0.101131	0.0505655	0.0101131	2.3562	1.1375	0.2717
40	80.05	30	8.05	0.9667599	0.00300455	2.29	1.16	0.24	0.1006913	0.0510052	0.0105528	2.4673	1.2008	0.3009
40	80.05	40	6.9	0.9612199	0.003505308	2.29	1.15	0.24	0.1006913	0.0505655	0.0105528	2.6764	1.3015	0.3102
40	80.05	50	5.75	0.9534639	0.00420637	2.28	1.17	0.25	0.1002516	0.0514449	0.0109925	2.9199	1.4608	0.366
40	80.05	51.3	5.6	0.9522217	0.00431904	2.28	1.16	0.26	0.1002516	0.0510052	0.0114322	3.0143	1.5106	0.392
	Initial Height (in)	12.5												
Nozzle (deg)	Mass (g)	Compression (%)	Height (in)	Porosity	Bulk Density (lb_fiber/in^3)	Flow Rate 0.075 ft/s (gpm)	Flow Rate 0.05 ft/s (gpm)	Flow Rate 0.01 ft/s (gpm)	Velocity 1 (ft/s)	Velocity 2 (ft/s)	Velocity 3 (ft/s)	DP 1 (psi)	DP 2 (ft/s)	DP 3 (ft/s)
40	120.04	0	12.5	0.9678995	0.002901549	1.7	1.13	0.24	0.074749	0.0496861	0.0105528	2.78492	1.84249	0.45399
40	120.04	10	11.25	0.9643327	0.003223943	1.7	1.17	0.23	0.074749	0.0514449	0.0101131	2.8124	1.8935	0.4332
40	120.04	20	10	0.9598743	0.003626936	1.71	1.16	0.22	0.0751887	0.0510052	0.0096734	2.9097	2.0001	0.4314
40	120.04	30	8.75	0.9541421	0.00414507	1.7	1.16	0.21	0.074749	0.0510052	0.0092337	3.1065	2.109	0.4653
40	120.04	40	7.5	0.9464991	0.004835915	1.7	1.15	0.24	0.074749	0.0505655	0.0105528	3.4275	2.2659	0.5754
	Initial Height (in)	8												
Nozzle (deg)	Mass (g)	Compression (%)	Height (in)	Porosity	Bulk Density (lb_fiber/in^3)	Flow Rate 0.1 ft/s (gpm)	Flow Rate 0.05 ft/s (gpm)	Flow Rate 0.01 ft/s (gpm)	Velocity 1 (ft/s)	Velocity 2 (ft/s)	Velocity 3 (ft/s)	DP 1 (psi)	DP 2 (psi)	DP 3 (psi)
15	40.09	0	8	0.9832489	0.001514119	2.3	1.15	0.24	0.101131	0.0505655	0.0105528	0.9225	0.4471	0.0987
15	40.09	10	7.2	0.9813877	0.001682354	2.31	1.14	0.22	0.1015707	0.0501258	0.0096734	0.9423	0.453	0.0977
15	40.09	20	6.4	0.9790612	0.001892649	2.29	1.13	0.22	0.1006913	0.0496861	0.0096734	0.9711	0.4644	0.1043
15	40.09	30	5.6	0.9760699	0.002163027	2.31	1.13	0.25	0.1015707	0.0496861	0.0109925	1.0422	0.4949	0.1208
15	40.09	40	4.8	0.9720816	0.002523532	2.31	1.17	0.24	0.1015707	0.0514449	0.0105528	1.1035	0.5507	0.1297
15	40.09	50	4	0.9664979	0.003028238	2.31	1.16	0.25	0.1015707	0.0510052	0.0109925	1.2253	0.6107	0.1421
15	40.09	70	2.4	0.9441631	0.005047063	2.31	1.13	0.25	0.1015707	0.0496861	0.0109925	1.5871	0.7642	0.1992
	Initial Height (in)	11.5												
Nozzle (deg)	Mass (g)	Compression (%)	Height	Porosity	Bulk Density (lb_fiber/in^3)	Flow Rate 0.1 ft/s (gpm)	Flow Rate 0.05 ft/s (gpm)	Flow Rate 0.01 ft/s (gpm)	Velocity 1 (ft/s)	Velocity 2 (ft/s)	Velocity 3 (ft/s)	DP 1 (psi)	DP 2 (psi)	DP 3 (psi)
15	79.99	0	11.5	0.9767494	0.002101608	2.3	1.16	0.24	0.101131	0.0510052	0.0105528	2.1845	1.0674	0.2328
15	79.99	10	10.35	0.974166	0.002333512	2.31	1.16	0.22	0.1015707	0.0510052	0.0096734	2.3656	1.128	0.2387
15	79.99	20	9.2	0.9709367	0.00262701	2.32	1.16	0.21	0.1020104	0.0510052	0.0092337	2.3285	1.1414	0.2464
15	79.99	30	8.05	0.9667849	0.003002298	2.3	1.16	0.24	0.101131	0.0510052	0.0105528	2.4111	1.2099	0.2832
15	79.99	40	6.9	0.961249	0.003502681	2.3	1.17	0.25	0.101131	0.0514449	0.0109925	2.6219	1.3217	0.3042
15	79.99	50	5.75	0.9534988	0.004203217	2.32	1.14	0.21	0.1020104	0.0501258	0.0092337	2.946	1.4306	0.3011
15	79.99	57.61	4.875	0.9451507	0.00495764	2.3	1.17	0.24	0.101131	0.0514449	0.0105528	3.2078	1.6221	0.3782
	Initial Height (in)	12.5												
Nozzle (deg)	Mass (g)	Compression (%)	Height	Porosity	Bulk Density (lb_fiber/in^3)	Flow Rate 0.075 ft/s (gpm)	Flow Rate 0.05 ft/s (gpm)	Flow Rate 0.01 ft/s (gpm)	Velocity 1 (ft/s)	Velocity 2 (ft/s)	Velocity 3 (ft/s)	DP 1 (psi)	DP 2 (psi)	DP 3 (psi)
15	120.04	0	12.5	0.9678995	0.002901549	1.7	1.13	0.24	0.074749	0.0496861	0.0105528	2.7306	1.8204	0.4062
15	120.04	10	11.25	0.9643327	0.003223943	1.7	1.17	0.23	0.074749	0.0514449	0.0101131	2.769	1.8266	0.3712
15	120.04	20	10	0.9598743	0.003626936	1.71	1.16	0.22	0.0751887	0.0510052	0.0096734	2.8664	1.8741	0.4265
15	120.04	30	8.75	0.9541421	0.00414507	1.7	1.16	0.21	0.074749	0.0510052	0.0092337	3.0107	2.0261	0.4263
15	120.04	40	7.5	0.9464991	0.004835915	1.7	1.15	0.24	0.074749	0.0505655	0.0105528	3.3225	2.2264	0.4968
	Initial Height (in)	8												
Nozzle (deg)	Mass (g)	Compression (%)	Height	Porosity	Bulk Density (lb_fiber/in^3)	Flow Rate 0.1 ft/s (gpm)	Flow Rate 0.05 ft/s (gpm)	Flow Rate 0.01 ft/s (gpm)	Velocity 1 (ft/s)	Velocity 2 (ft/s)	Velocity 3 (ft/s)	DP 1 (psi)	DP 2 (psi)	DP 3 (psi)
40	40.06	0	8	0.9832615	0.001512986	2.32	1.14	0.25	0.1020104	0.0501258	0.0109925	0.8314	0.3913	0.0941
40	40.06	10	7.2	0.9814016	0.001681095	2.28	1.14	0.22	0.1002516	0.0501258	0.0096734	0.8321	0.4028	0.088
40	40.06	20	6.4	0.9790768	0.001891232	2.31	1.14	0.24	0.1015707	0.0501258	0.0105528	0.8838	0.4215	0.1036
40	40.06	30	5.6	0.9760878	0.002161408	2.29	1.13	0.25	0.1006913	0.0496861	0.0109925	0.9191	0.4473	0.1126
40	40.06	69.38	2.45	0.9453347	0.004940362	2.3	1.13	0.23	0.101131	0.0496861	0.0101131	1.4743	0.7082	0.1732

A.3 Mechanical Loading Response Results

The results from the Mechanical Loading Response test can be seen below.

40 degree

Bed 1 mass (g)	120.06								Apparatus	Mass (g)	Weight (lb)
Bed 2 mass (g)	120.07								comp screen assm	440.28	0.9707
Bed 3 mass (g)	120.01								weight holder	469.41	1.0349
									Screen Bouyant Force		0.2526
		Bed 1			Bed 2			Bed 3			
Mass of Weights (lbs)	Weight(screen subtracted)	Bed Height	Deflection	Bulk Density (lb/in^3)	Bed Height	Deflection	Bulk Density (lb/in^3)	Bed Height	Deflection	Bulk Density (lb/in^3)	Average Density
0	0	23.5	0	0.001543634	24.5	0	0.001480752	19.5	0	0.001859502	0.001627963
0.9707	0.7181	18.25	5.25	0.001987693	22	2.5	0.001649019	17.375	2.125	0.002086924	0.001907879
2.0056	1.753	17	6.5	0.002133847	20.5	4	0.001769679	16.875	2.625	0.002148758	0.002017428
3.0056	2.753	16.125	7.375	0.002249638	19.375	5.125	0.001872435	16.125	3.375	0.002248701	0.002123591
4.0056	3.753	15.5	8	0.002340349	18.375	6.125	0.001974336	15.75	3.75	0.002302241	0.002205642
5.0056	4.753	15.125	8.375	0.002398374	17.625	6.875	0.00205835	15.25	4.25	0.002377724	0.00227815
7.0056	6.753	14.25	9.25	0.002545642	16.375	8.125	0.002215476	14.75	4.75	0.002458325	0.002406481
9.0056	8.753	13.625	9.875	0.002662415	15.375	9.125	0.002359572	14.375	5.125	0.002522456	0.002514814
11.0056	10.753	13.5	10	0.002687067	14.875	9.625	0.002438886	14.25	5.25	0.002544582	0.002556845
16.0056	15.753							13.625	5.875	0.002661306	
21.0056	20.753							12.625	6.875	0.002872103	
26.0056	25.753							12.625	6.875	0.002872103	
	OLD										
Bed 1 Mass (g)	119.96										
Bed 2 Mass (g)	119.81										
Bed 3 Mass (g)	120.1										
Mass of Weights (lbs)	Weight(screen subtracted)	Bed Height	Deflection	Bulk Density (lb/in^3)	Bed Height	Deflection	Bulk Density (lb/in^3)	Bed Height	Deflection	Bulk Density (lb/in^3)	Average Density
0	0	17.5	0	0.002071154	20	0	0.001809993	16.25	0	0.002231403	0.002037517
0.9707	0.7181	16.25	1.25	0.002230473	17.875	2.125	0.002025168	15.25	1	0.002377724	0.002211122
2.0056	1.753	15.375	2.125	0.002357411	16.75	3.25	0.002161186	14.75	1.5	0.002458325	0.002325641
3.0056	2.753	15	2.5	0.002416346	16	4	0.002262492	14.375	1.875	0.002522456	0.002400431
4.0056	3.753	14.5	3	0.002499668	15.8	4.2	0.002291131	14	2.25	0.002590021	0.002460274
5.0056	4.753	14.125	3.375	0.002566031	15.125	4.875	0.00239338	13.625	2.625	0.002661306	0.002540239
7.0056	6.753	13.5	4	0.002684829	14.5	5.5	0.002496543	13.125	3.125	0.002762689	0.00264802
9.0056	8.753	13	4.5	0.002788092	14.375	5.625	0.002518252	12.75	3.5	0.002843945	0.002716763
11.0056	10.753	12.75	4.75	0.00284276	13.25	6.75	0.002732066	12.375	3.875	0.002930125	0.002834984
16.0056	15.753	12.25	5.25	0.002958791	13	7	0.002784605	11.625	4.625	0.003119165	0.002954187
21.0056	20.753	12.125	5.375	0.002989294	12.625	7.375	0.002867316	11.125	5.125	0.003259353	0.003038654
26.0056	25.753	12.125	5.375	0.002989294	12.375	7.625	0.002925242	10.25	6	0.00353759	0.003150709
Bed 1 Mass (g)	120.28										
Bed 2 Mass (g)	120.42										
		Test 08272013 3:30			Test 08272013 4:15						
Mass of Weights (lbs)	Weight(screen subtracted)	Bed Height	Deflection	Bulk Density (lb/in^3)	Bed Height	Deflection	Bulk Density (lb/in^3)	Bed Height	Deflection		
0	0	14.75	0	0.002463856	14.75	0	0.002466724		16.25		
0.9707	0.7181	14	0.75	0.002595848	14.25	0.5	0.002553276		16.25		
2.0056	1.753	13.625	1.125	0.002667294	13.875	0.875	0.002622283		16.25		
3.0056	2.753	13.25	1.5	0.002742783	13.625	1.125	0.002670398		16.25		
4.0056	3.753	13	1.75	0.002795529	13.375	1.375	0.002720312		16.25		
5.0056	4.753	12.75	2	0.002850343	13.125	1.625	0.002772128		16.25		
7.0056	6.753	12.375	2.375	0.002936717	12.625	2.125	0.002881915		16.25		
9.0056	8.753	12	2.75	0.00302849	12.25	2.5	0.002970137		16.25		
11.0056	10.753	11.625	3.125	0.003126183	12	2.75	0.003032015		16.25		
16.0056	15.753	10.75	4	0.00338064	11.125	3.625	0.003270488		16.25		
21.0056	20.753	10	4.75	0.003634188	10.375	4.375	0.003506909		16.25		
26.0056	25.753	9.125	5.625	0.003982671	9.25	5.5	0.003933425		16.25		

A.4 Flow Induced Compression of an NEI Fiber Bed Results

The results from the Flow Induced Compression test can be seen below.

			Test 1										
height	mass	velocity	lin den	DP1	DP2	DP3	DP4	DP5	DP6	DP7	DP8	DP9	DP10
0.889	0.08004	0.033417	0.090034	-99.6696	31.14675	62.2935	31.14675	31.14675	31.14675	62.2935	62.2935	124.587	-62.2935
0.8128	0.08004	0.057161	0.098474	105.899	218.0273	62.2935	124.587	218.0273	93.44025	186.8805	31.14675	218.0273	93.44025
0.6096	0.08004	0.071671	0.131299	407.3995	404.9078	218.0273	373.761	342.6143	186.8805	311.4675	404.9078	404.9078	155.7338
0.52705	0.08004	0.086621	0.151864	878.3384	591.7883	685.2285	560.6415	560.6415	436.0545	716.3753	498.348	249.174	249.174
0.47625	0.08004	0.101571	0.168063	1333.081	809.8155	996.696	996.696	467.2013	1027.843	778.6688	404.9078	404.9078	249.174
0.4445	0.08004	0.110365	0.180067	1669.466	1214.723	1058.99	1308.164	809.8155	1277.017	622.935	498.348	280.3208	373.761
0.403225	0.08004	0.124875	0.1985	2360.924	1775.365	1495.044	1277.017	1899.952	1152.43	716.3753	436.0545	436.0545	155.7338
0.37465	0.08004	0.137186	0.213639	3077.299	2367.153	2055.686	1557.338	2242.566	1121.283	685.2285	747.522	280.3208	560.6415
			Test 2										
height	mass	velocity	lin den	DP1	DP2	DP3	DP4	DP5	DP6	DP7	DP8	DP9	DP10
0.9271	0.08003	0.032978	0.086323	93.44025	62.2935	31.14675	62.2935	93.44025	-62.2935	31.14675	93.44025	62.2935	0
0.6477	0.08003	0.059799	0.12356	560.6415	186.8805	249.174	93.44025	186.8805	124.587	155.7338	124.587	93.44025	155.7338
0.517525	0.08003	0.079146	0.15464	1189.806	498.348	404.9078	436.0545	373.761	311.4675	311.4675	529.4948	498.348	93.44025
0.4318	0.08003	0.098053	0.18534	1956.016	965.5493	747.522	903.2558	498.348	716.3753	965.5493	404.9078	467.2013	280.3208
0.3937	0.08003	0.111244	0.203277	2585.18	1401.604	1090.136	1152.43	809.8155	1339.31	591.7883	654.0818	436.0545	685.2285
0.352425	0.08003	0.126634	0.227084	3382.537	1899.952	1432.751	1526.191	1619.631	1308.164	654.0818	778.6688	903.2558	622.935
0.3302	0.08003	0.133669	0.242368	3918.261	2211.419	1931.099	1619.631	2024.539	1152.43	934.4025	716.3753	1027.843	436.0545
0.29845	0.08003	0.156094	0.268152	4921.187	3706.463	2927.795	2491.74	2304.86	1463.897	996.696	1339.31	654.0818	685.2285
			Test 3										
height	mass	velocity	lin den	DP1	DP2	DP3	DP4	DP5	DP6	DP7	DP8	DP9	DP10
0.93345	0.08003	0.035176	0.085736	155.7169	93.43013	62.28675	62.28675	31.14338	62.28675	93.43013	62.28675	62.28675	62.28675
0.6858	0.08003	0.065076	0.116696	797.2704	342.5771	280.2904	342.5771	373.7205	249.147	93.43013	62.28675	249.147	124.5735
0.631825	0.08003	0.087061	0.126665	1239.506	591.7241	373.7205	591.7241	591.7241	249.147	62.28675	280.2904	311.4338	124.5735
0.5588	0.08003	0.107727	0.143218	2030.548	1027.731	778.5844	1058.875	622.8675	93.43013	529.4374	467.1506	529.4374	218.0036
0.508	0.08003	0.127513	0.157539	2915.02	1370.309	1339.165	1494.882	342.5771	685.1543	685.1543	218.0036	747.441	467.1506
0.47625	0.08003	0.141144	0.168042	3656.232	1899.746	1744.029	1681.742	654.0109	903.1579	1058.875	654.0109	342.5771	249.147
0.4318	0.08003	0.153016	0.18534	4397.445	2491.47	2273.466	1494.882	1121.162	1152.305	965.4446	778.5844	342.5771	62.28675
0.381	0.08003	0.180717	0.210052	7150.519	3768.348	3270.054	1837.459	1712.886	1526.025	934.3013	529.4374	186.8603	280.2904

A.5 Porosity Distribution due to Variable Velocity

The results from the Porosity Distribution test can be seen below.

		zero	5.375	5.375	5.375	5.375	5.375	5.375	5.375	5.375	5.375	5.375	5.375	5.375	5.375	5.375	5.375		Divider Height			
flow rate	bed height	DP	p1	p2	p3	p4	p5	p6	p7	p8	p9	p10	p11	p12	p13	p14	p15	#1	#2	#3	#4	#5
2.28	22.75	20.125	20	19	18.125	17.75	16.625	15	14	12.625	12	11.25	10.125	9.25	8.75	8	7.125	2.25	5	8.125	10.5	14.375
2.63	19.75	29.5	26.25	25.125	24	21.75	19	17	14.875	13.75	12.625	10.625	9.75	8.625	7.375	6.75	6	1.875	3.875	6.625	8.75	12.375
2.92	17.75	38.56	32.625	30.25	28.25	24.625	20.5	17.625	15.875	14.625	11.25	10.5	8.875	7.25	6.375	6.25	6.125	1.625	3.25	5.875	7.75	11.125
3.3	16	49.77	41	37.625	33	27.375	22.25	18.875	17.25	12.75	11.5	9.5	7.625	6.675	6.25	6	5.5	1.375	2.75	5.25	7	9.75
3.9	14	72.3	57.25	49	40.5	31.25	24.375	20.875	13.875	12.25	8.375	7	6.375	6	5.25	5.125	5	1.25	2.375	4.375	5.75	8.375

Appendix B

Curve Fitting

B.1 Linear Density Fit

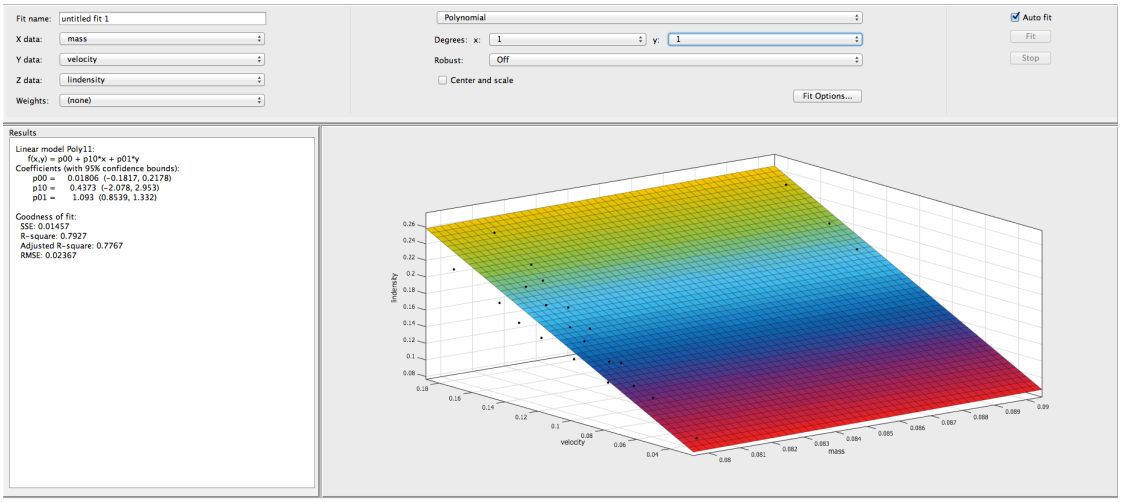

B.2 Porosity Fit